

Stability analysis of singular patterns in the 1-D Gray–Scott model I: A matched asymptotics approach

Arjen Doelman
Mathematisch Instituut, Universiteit Utrecht
P.O. Box 80.010, 3508TA Utrecht, The Netherlands

Robert A. Gardner
Department of Mathematics, University of Massachusetts
Amherst, MA 01003, U.S.A.

Tasso J. Kaper
Department of Mathematics, Boston University
Boston, MA 02215, U.S.A.

September 26, 1997

Abstract

In this work, we analyze the linear stability of singular homoclinic stationary solutions and spatially-periodic stationary solutions in the one-dimensional Gray-Scott model. This stability analysis has several implications for understanding the recently discovered phenomena of self-replicating pulses. For each solution constructed in [5], we analytically find a large open region in the space of the two scaled parameters in which it is stable. Specifically, for each value of the scaled inhibitor feed rate, there exists an interval, whose length and location depend on the solution type, of values of the activator (autocatalyst) decay rate for which the solution is stable. The upper boundary of each interval corresponds to a subcritical Hopf bifurcation point, and the lower boundary is explicitly determined by finding the parameter value where the solution ‘disappears,’ *i.e.*, below which it no longer exists as a solution of the steady state system. Explicit asymptotic formulae show that the one-pulse homoclinic solution gains stability first as the second parameter is decreased, and then successively, the spatially periodic solutions (with decreasing period) become stable. Moreover, the stability intervals for different solutions overlap. Explicit determination of these stability intervals plays a central role in understanding pulse self-replication. Numerical simulations confirm that the spatially periodic stationary solutions are attractors in the pulse-splitting regime; and, moreover, whenever, for a given solution, the value of the activator decay rate was taken to lie in the regime below that solution’s stability interval, initial data close to that solution was observed to evolve toward a different spatially periodic stationary solution, one whose stability interval included the parameter value. The main analytical technique used is that of matched asymptotic expansions.

1 Introduction

The irreversible Gray–Scott model [14, 15, 16] is governed by the equations:

$$\begin{aligned}\frac{\partial U}{\partial t} &= \nabla^2 U - UV^2 + A(1 - U), \\ \frac{\partial V}{\partial t} &= D\nabla^2 V + UV^2 - BV.\end{aligned}\tag{1.1}$$

Here $U = U(x, t)$ and $V = V(x, t)$ denote the concentrations of the two chemical species \mathcal{U} and \mathcal{V} , ∇^2 denotes the Laplacian, D is the normalized diffusivity of \mathcal{V} , A denotes the rate at which \mathcal{U} is fed from the reservoir into the reactor, and B is the overall rate of decay of \mathcal{V} . See also [2] for a thorough analysis of the reaction kinetics in the spatially homogeneous case.

It has recently been discovered that the Gray-Scott system exhibits self-replicating spots in two dimensions [27], [22], and [21] and self-replicating pulses in one space dimension [29] and [28]; see also [30] and [5]. A spot in two space dimensions (and similarly a pulse in one dimension) was loosely defined as a region (interval) of high V and low U . Outside of such a region (interval), the concentrations are essentially those of the globally stable homogeneous steady state: *i.e.*, U is near one and V is extremely close to zero. There exist large regions of the $A - B - D$ parameter space in which spots (pulses) deform (widen) until they split into two spots (pulses), and this process repeats itself until any one of a variety of time asymptotic states is reached [27].

In one space dimension, the focus has been on the case in which D is small: $D = \delta^2 \ll 1$, [29], [28], and [30], and the parameters A and B are small, $\ll 1$, [29], [30] and [5]. In particular, in [5] the parameters scale as $A = \delta^2 a$, and $B = \delta^\beta b$, where $0 \leq \beta < 1$ and where $a, b = \mathcal{O}(1)$ with respect to δ :

$$\begin{aligned}\frac{\partial U}{\partial t} &= \frac{\partial^2 U}{\partial x^2} - UV^2 + \delta^2 a(1 - U), \\ \frac{\partial V}{\partial t} &= \delta^2 \frac{\partial^2 V}{\partial x^2} + UV^2 - \delta^\beta bV,\end{aligned}\tag{1.2}$$

where $x \in \mathbf{R}$. It is crucial for the analysis in this paper to *not* a priori fix the value of β , *i.e.* the magnitude of B : we will find that both the existence and the stability of the singular patterns studied in this paper depend non-trivially on the value β .

Typical one-pulse data in the splitting regime rapidly broaden and split into two slowly ($\ll 1$) traveling pulses. These left and right moving pulses self-replicate after time intervals ($\gg 1$) sending new pulses into the interior of the interval, while the outer pulses travel on, without changing speed. Both the velocity of the pulses and the ‘waiting time’ until the next self-replicating event depend on the magnitude of B (or β), see [5] and [4]. In turn, both the inner pulses and the outer pulses can split again, although this can also depend on the length of the interval. However, as the reaction progresses, those pulses which no longer self-replicate (*i.e.*, those pulses that are sufficiently deep inside the interval) are observed during the numerical simulations to align themselves in spatially periodic stationary patterns [29] and [5]. In this way, the spatially periodic stationary patterns, whose existence was demonstrated analytically in [5], act as attractors in the self-replicating pulse domain.

Another significant numerical observation reported in [5] is that there exists a transition regime in which stationary, one-pulse homoclinic solutions are stable. This regime constitutes a transition

regime between the parameter combinations (above it) for which pulse-like data decays to the spatially homogeneous steady state ($U \equiv 1, V \equiv 0$) and the pulse-splitting regime (below it), where pulse-like data undergoes the splitting process just described. The existence of these one-pulse solutions (and also of multiple pulse homoclinic orbits) for all $\mathcal{O}(1)$ pairs of a and b in the partial differential equation (1.2) was demonstrated in [5].

Since the stationary, spatially periodic singular solutions and the stationary one-pulse homoclinic solutions established in [5] play central roles in the self-replication process, we have conducted a thorough investigation of their stability. In this work, which is the first part of a pair of papers, we perform a singular perturbation analysis using matched asymptotic expansions of the stability of all of these solutions. In second part, see [6], we present the rigorous mathematical analysis that justifies the formal work for the one-pulse homoclinic solutions presented in this paper and sheds significant light on the entire stability analysis.

Our principal analytical findings in this part are as follows. For each of the stationary solutions, and for each $A = \mathcal{O}(\delta^2)$, there exists an interval of B values depending on a and the type of the solution (in particular, the period \mathcal{T} or the distance between pulses) in which the solution is stable. The upper boundary, B_H , of each interval scales as $B_H = b_H \sqrt{\delta}$, where $b_H = \mathcal{O}(1)$ with respect to δ , *i.e.* $\beta = \frac{1}{2}$ in (1.2). It is determined by a Hopf bifurcation. We can explicitly show that critical scaling is $b_H \approx K \sqrt{a}$, where K depends on the solution type, and for example $K \approx 0.66$ for stationary one-pulse homoclinic solutions (at leading order). Moreover, the Hopf bifurcation is subcritical. For $B > B_H$, the stationary solution is unstable; there are either two distinct positive real eigenvalues (for $B > B_C = \sqrt{\delta} b_C$ which depends on a and the solution type) or a complex conjugate pair of eigenvalues with positive real part (for $B_C < B < B_H$). Whereas, for $B < B_H$, it is stable and there also exists an unstable oscillatory solution that bifurcated off of the stationary solution.

The lower boundary, B_D , of each interval scales as $B_D = b_D \delta$, where $b_D = \mathcal{O}(1)$, *i.e.* $\beta = 1$ in (1.2). We show using topological shooting that the B_D correspond to the parameter values at which the solutions of the associated fourth order system of ordinary differential equations [5] cease to exist, *i.e.*, they disappear. In addition, based on numerical simulations, we observe that the value of B_D coincides with the upper boundary of the splitting regime.

On a bounded (and long) interval $[0, L]$, ($L \gg 1$) (with homogeneous Neumann boundary conditions), a periodic solution of (1.2) with spatial period \mathcal{T} is represented by an N -pulse pattern, where N is determined by \mathcal{T} and L . The explicit formulae for the stability intervals reveal that, for each $A = \mathcal{O}(\delta^2)$, the stability intervals of the one-pulse homoclinic and N -pulse spatially periodic solutions overlap for a sequence of adjacent N values. Moreover, it follows from the theory developed in this paper that, for fixed $A = \delta^2 a$ and decreasing B , the one-pulse homoclinic pattern is the first to become stable, followed by the 2-pulse pattern, 3-pulse pattern, etc.

The stationary one-pulse homoclinic solutions and family of stationary, spatially periodic solutions constructed in [5] are all singular in the limit $\delta \rightarrow 0$. For each pulse, the maximum of V (*i.e.*, the pulse height) scales as an inverse power of δ , $\delta^{-\frac{1}{2}\beta}$, while its width vanishes as $\delta \rightarrow 0$. In addition, there is a jump discontinuity in the first derivative U_x at the center of the pulse, with $U \sim \delta^{\frac{3}{2}\beta}$, in the limit $\delta \rightarrow 0$, see Figure 2. The singular structure was analyzed using geometric singular perturbation theory [19]. The theory could only be applied for $0 \leq \beta < 1$, although see Remark 1.1, and we note that the parameter β here is equivalent to the parameter $2\alpha/3$ from [5].

It was shown that a pulse lies near the homoclinic orbit of the fast reduced subsystem, and has an asymptotic expansion referred to as a fast (or inner) solution. By contrast, the solution segments outside of the pulse intervals lie close to slow manifolds, and have asymptotic expansions referred to as slow (or outer) solutions.

Given the singular structure of the one-pulse and spatially-periodic stationary patterns, as just described, their linear stability analysis is carried out as follows. First, we determine the relevant scalings of the eigenvalues (discrete spectrum): based on an asymptotic analysis presented in the Appendix, we show that there can only be unstable eigenvalues λ , *i.e.* $\text{Re}(\lambda) \geq 0$, for $\lambda = \mathcal{O}(\delta^\beta)$ with $\beta \in [0, 1)$ and for $\lambda = \mathcal{O}(\delta^{1-\beta})$ with $\beta \in [0, \frac{1}{2}]$. Second, we explicitly reduce the fourth-order eigenvalue problem to a nonlocal second-order eigenvalue problem, referred to as the NLEP. This reduction is achieved by exploiting the fast-slow (inner-outer) structure of the bounded unstable eigenfunctions, which is similar to that of the underlying stationary waves (*i.e.*, slow segments over the same x -intervals and fast segments over the same stretched x -intervals) in the parameter regimes where they exist. We construct the eigenfunctions using matched asymptotic expansions, and the central feature is that the derivative of the first-component of the eigenfunction has a jump discontinuity at the center of the pulse in the limit as $\delta \rightarrow 0$, just as U_x did for the wave itself. Matching the values of this jump discontinuity from both the fast and the slow fields leads to the NLEP. Now, the NLEP has a homogeneous part that is precisely the eigenvalue problem for the fast reduced homoclinic solution, but it also has a nonlocal inhomogeneous term that explicitly encodes the coupling of the slow field into the fast field. This inhomogeneous term is of $\mathcal{O}(\delta^{1-2\beta})$ for $0 \leq \beta \leq \frac{1}{2}$ and $\mathcal{O}(1)$ for $\frac{1}{2} \leq \beta < 1$. Finally, using hypergeometric functions, we are able to explicitly search for eigenvalue-eigenfunction pairs in the NLEP for which the real part of the eigenvalue is positive and the associated eigenfunction is bounded at infinity. In this way, we analytically determine the above mentioned bifurcation values b_C and b_H , and conduct a complete linear stability analysis.

On the one hand, the above stability and disappearance results also have a natural interpretation in the context of the singular perturbation structure of (1.2). The homoclinic orbit of the fast field, which is the well known Fisher-KPP equation, contributes one positive eigenvalue to the wave's spectrum, and normally such an eigenvalue renders the solution of the full problem unstable, see [17]. Indeed, this is the case when $B > B_C = b_c\sqrt{\delta}$, because then the coupling of the slow field to the fast field is insufficiently strong, *i.e.* the inhomogeneous term in the NLEP is too small, to qualitatively change the spectrum. Notably, however, when B decreases from B_C to B_H , the strength of this coupling increases, so that this fast instability has been removed for $B_D < B < B_H$, and the wave is stable in this interval.

On the other hand, it is also possible to study the stability of the singular one-pulse patterns with the Evans function, and an attendant homotopy invariant called the *stability index* (see e.g. [1], [13], [18]). The stability index detects the unstable eigenvalue of the homoclinic Fisher-KPP wave, which would seem to preclude the possibility of the perturbed wave becoming stable. This is called the '*NLEP paradox*' in the second part of this paper, [6]: how can a solution that approximates as $\delta \rightarrow 0$ an unstable solution of the fast reduced limit regain stability as a solution of the full system? This question is resolved in [6] through a careful analysis of the NLEP equation, which is shown to contribute a *pole* at the exact location of the unstable eigenvalue of the Fisher-KPP wave, which cancels the extraneous "eigenvalue" in the index calculation. The stability of the perturbed wave is therefore shown to be determined by the location of the other eigenvalues of the NLEP equation.

Another issue that needed to be addressed in order to make the stability analysis completely rigorous is to precisely determine the number of eigenvalues in a full neighborhood of the origin. This is complicated by the presence of the continuous spectrum of the wave, since it approaches the origin for small δ . In this case, the main tracking lemma used to construct the stability index breaks down. This obstacle is overcome by a new construction, in which the Evans function and the stability index are continued into the continuous spectrum and lifted to a Riemann surface, see [6] for details.

Reynolds, Ponce-Dawson and Pearson [29] and [30] also construct one-pulse and N -pulse spatially periodic solutions for the one-dimensional Gray-Scott model with $D = \delta^2 \ll 1$, although without scaling A and B . They match inner solutions, describing the pulses, and outer solutions, describing those segments of the solutions where V is very small and U changes slowly (namely, in the intervals exterior to the pulses). Their construction exploits the flux of U into the pulses through their sides. Using a ‘fuel and fire picture’ in which U denotes the fuel concentration and V denotes the fuel temperature, they state: “the lateral or diffusive feed of fuel (U) into the sides of the pulses ... is essential since the external feed (represented by the A term) is not sufficient by itself to keep the fire burning.” Imbalances between the flux into the pulse from the left and right sides cause the pulse to move. They develop asymptotic approximations for the variable pulse speeds in terms of the lateral flux, as well as predictions for when pulse-splitting occurs. Their analysis also suggests the presence of overlapping stability intervals, as is shown here. Finally, they generalize their results to include Gray-Scott like models wherein the nonlinear term consists of different terms of the form $U^{p_1}V^{p_2}$.

The paper is organized as follows. In section 2, we briefly summarize the existence results for the stationary solutions obtained in [5] that is needed for analyzing their stability. The main stability results are stated in section 3. In sections 4 and 5, the full fourth order eigenvalue problem is reduced to a second order nonlocal problem (NLEP) and this nonlocal equation is studied. Then, in section 6, we analyze the disappearance of the one-pulse solutions for small B . Finally, in section 7, we report a series of numerical simulations that corroborate the matched asymptotic analysis presented in the earlier sections, and we conclude in section 8 with a discussion.

Remark 1.1. The results of [5] have been extended to a much larger region in the A, B, D parameter space of the general equation (1.1) in [4]. There, we show that if $B^3D \leq A \ll B^2$, then the method used to construct the homoclinic and spatially periodic stationary solutions for (1.2) in [5] also directly yields the existence of these solutions in the original, unscaled Gray-Scott model. Note therefore that, while sufficient, the scalings $A = \mathcal{O}(\delta^2)$ and $B = \mathcal{O}(\delta^\beta)$, $\beta \in [0, 1)$, are not necessary, contrary to the ‘must scale’ claim in the Introduction of [5].

2 Single pulse and spatially periodic stationary patterns

The spatially homogeneous steady state ($U(x, t) \equiv 1, V(x, t) \equiv 0$) is globally stable under the dynamics of the governing equation (1.2). We denote it by S . The single pulse homoclinic steady states considered here connect S to itself as $x \rightarrow \pm\infty$. Moreover, in a narrow interval centered at $x = 0$, they make a large excursion away from the homogeneous steady state during which V is large and U is small. The spatially periodic steady states considered here have large wavelength, and each periodic segment lies near the single pulse homoclinic steady state.

Time independent solutions of the partial differential equation (1.2), such as the steady states under study here, satisfy the coupled system of ordinary differential equations obtained from (1.2) by setting $U_t, V_t = 0$. In [5], the following scaled system of ordinary differential equations was derived (see equation (2.5) there):

$$\begin{aligned} u_{\xi\xi} &= \delta^{2(1-\beta)} \left(uv^2 - \delta^{2-\frac{1}{2}\beta} a + \delta^{2+\beta} au \right) \\ v_{\xi\xi} &= -uv^2 + bv, \end{aligned} \tag{2.1}$$

with $0 \leq \beta < 1$. Here, the subscript ξ denotes $d/d\xi$; we explicitly set $c = \gamma = 0$; the following scalings were used:

$$A = \delta^2 a, B = \delta^\beta b, x = \delta^{1-\frac{1}{2}\beta} \xi, U \rightarrow \delta^{\frac{3}{2}\beta} u, V \rightarrow \delta^{-\frac{1}{2}\beta} v; \tag{2.2}$$

and, finally, the parameter β is equivalent to the ratio $2\alpha/3$ from [5]. The scalings given by (2.2) were introduced in [5] because in the original variables, the V -pulse is of $\mathcal{O}(\delta^{-\frac{1}{2}\beta}) \gg 1$ height (and is of $\mathcal{O}(\delta^{1-\frac{1}{2}\beta})$ width) while U attains a minimum of $\mathcal{O}(\delta^{\frac{3}{2}\beta})$ at the center of the pulse. (Note that the parameter β here is not related to the β of [5], and no confusion can arise since there β was used to scale the wave speed in the search for traveling waves with $c \neq 0$.) The homoclinic and spatially periodic stationary solutions with one or multiple pulses were constructed in [5] using methods from geometric singular perturbation theory; see [10] and [19] for original treatments of this theory.

2.1 Single pulse homoclinic solutions

The system of ordinary differential equations (2.1) has a saddle-saddle fixed point at $(u = 1, u_\xi = 0, v = 0, v_\xi = 0)$, which corresponds precisely to the homogeneous steady state S of (1.2). We shall also use S to label it here, despite the abuse of notation. The point S lies on the two-dimensional plane $\mathcal{M} \equiv (u, u_\xi, v = 0, v_\xi = 0)$ that is an invariant slow manifold for (2.1).

The existence of single pulse stationary states biasymptotic to S was established via the following theorem (see Theorems 4.1 and 4.3 of [5] as well as section 5 for the nonexistence result when $c \neq 0$):

Theorem 1. There exists a $\delta_0(\beta)$ such that for every $0 < \delta < \delta_0(\beta)$ and $0 < \beta < 1$, the system (2.1) has a unique one-pulse orbit $\Gamma_1(\xi; a, b, \delta)$ homoclinic to S . When $\beta = 0$, there exist two orbits homoclinic to S . Moreover, in the five-dimensional system of first-order ordinary differential equations obtained from (2.1) by appending the trivial equation $c_\xi = 0$ for the wave speed c , these orbits lie in the transverse intersection of $W^u(S)$ and $W^s(S)$ at $c = 0$.

The single pulse homoclinic solutions Γ_1 given by Theorem 1 consist of clearly distinguished slow and fast segments. In the phase space interpretation (Figures 1a and 2), there are two slow segments during which the homoclinic orbit is exponentially close to the stable and unstable manifolds, respectively, of S restricted to the slow manifold \mathcal{M} , and there is a fast segment in between these slow segments during which the homoclinic orbit makes a large amplitude excursion away from \mathcal{M} : V is large while U is small. This excursion or ‘jump’ will also be referred to as a singular v -pulse (Figure 1).

More precisely, fixing the parametrizations of the orbits Γ_1 such that they are symmetric about $\xi = 0$, there exists a large value of ξ , call it Ξ , such that for all $-\Xi < \xi < \Xi$, the u -component of

the one-pulse homoclinic solution is constant to leading order:

$$u_0 = 3b\sqrt{\frac{b}{a}} + \text{h.o.t.}, \quad (2.3)$$

where $\Xi = \mathcal{O}(\delta^{-1/2})$ as $\delta \rightarrow 0$. In addition, the v -component of the one-pulse solution is described by

$$v_0(\xi) = \frac{3b}{2u_0} \text{sech}^2\left(\frac{\sqrt{b}\xi}{2}\right) + \mathcal{O}(\delta^{1-\beta}), \quad (2.4)$$

where the higher order terms also vanish exponentially as $\xi \rightarrow \pm\infty$. The leading order term is a solution of the conservative second-order equation: $v_{\xi\xi} = -u_0v^2 + bv$, which is obtained from (2.1) in the singular limit $\delta \rightarrow 0$. Combining (2.3) and (2.4) on the interval $(-\Xi, \Xi)$, we find:

$$v_0(\xi) = \frac{1}{2}\sqrt{\frac{a}{b}} \text{sech}^2\left(\frac{\sqrt{b}\xi}{2}\right) + \mathcal{O}(\delta^{1-\beta}). \quad (2.5)$$

More detailed information about the slow segments is also useful for this work. There exists a small finite value of x , call it X , such that outside of the interval $[-X, X]$, the homoclinic solution is $\mathcal{O}(e^{-c/\delta^{1-\beta}})$ close to the stable and unstable manifolds of the fixed point S restricted to the slow manifold \mathcal{M} . These ‘outer’ or slow regimes are governed to leading order by the linear equation

$$U_{xx} = \delta^2 a(1 - U), \quad (2.6)$$

which describes the flow in the slow manifold \mathcal{M} . This linear equation is obtained from (1.2) by setting $u_t = 0$ and by using the fact that the V -component of the homoclinic solutions is exponentially small for $|x| \geq X$. The restricted stable and unstable manifolds are straight lines labeled ℓ^s and ℓ^u , respectively, in Figure 1, and while the one-pulse state remains near them, U slowly changes between $\delta^{\frac{3}{2}\beta}u_0$ and 1, where u_0 is given by (2.3).

Remark 2.1. The fact that the intersection in Theorem 1 is transverse in the five-dimensional space at $c = 0$ is useful for the stability analysis. In particular, it will lead us to the conclusion that the eigenvalue at the origin of the complex eigenvalue plane, that corresponds to translation of the wave, is simple.

Remark 2.2. The system (2.1) is more degenerate than the usual fast-slow systems. While the fast subsystem captures the homoclinic pulse, not only can it not be used to describe the slow dynamics, as is usually the case, but the fixed point S on the slow manifold to which the orbit is homoclinic moves off to infinity in the u direction as $u|_S = \delta^{-\frac{2}{3}\beta}$. By contrast, in the slow system, the fixed point S is located at a finite point ($U = 1$), but the magnitude of the homoclinic excursion becomes unbounded, since $V \sim \delta^{-\frac{1}{2}\beta}$. This is important for the stability analysis.

Remark 2.3. On the manifold \mathcal{M} , U depends slowly on on the slow variable x , due to the scaling of $A = \delta^2 a$. Thus, $U(x)$ is ‘doubly slow’, since it even evolves slowly in the slow coordinate x . This yields that the periodic patterns have an $\mathcal{O}(\frac{1}{\delta})$ period, or, equivalently, the V -pulses are $\mathcal{O}(\frac{1}{\delta})$ apart, see Figures 1b, 2b and subsection 2.2. This property is also of crucial importance in the stability analysis of all of the stationary states.

2.2 Multiple pulse, spatially periodic stationary states

The linear outer equation (2.6) also has a one parameter family of hyperbolic cosine solutions that lie inside/below the wedge on \mathcal{M} formed by ℓ^u and ℓ^s , see Figure 1b. These solutions each attain a unique maximum value U_{\max} of U such that $U_{\max} < 1$, and they approach the asymptotes ℓ^u and ℓ^s of the family of hyperbolic cosine solutions as $x \rightarrow \pm\infty$, respectively. For describing as we do in this section a spatially periodic steady state of (1.2) with given values of a and b and with period \mathcal{T} , we are interested in a finite, symmetric segment of a particular hyperbola on \mathcal{M} that is obtained by flowing the maximal point (where $U = U_{\max}$) forward and backward under (2.6) for intervals of length $\mathcal{T}/2$ in the x variable. See Figure 2b, and we refer the reader to section 4.2 of [5] for further properties.

The existence of multiple-pulse, spatially periodic stationary states of (1.2) was established via the following theorem (see section 4.2 of [5]):

Theorem 2. For every δ sufficiently small and for $0 < \beta < 1$, there exists a family of spatially periodic steady states $\Gamma_m(\xi; a, b, \delta)$ of (1.2), parametrized by $m > 1$, such that each periodic state

(i) has a well-defined period of length

$$\mathcal{T}(m, a, b) = \frac{2}{\delta\sqrt{a}} \log \frac{m+1}{\sqrt{m^2-1}} + \text{h.o.t.} \quad (2.7)$$

(ii) consists of infinitely many copies a principal segment that is exponentially close to a hyperbolic cosine solution on \mathcal{M} for $x \in [-\frac{\mathcal{T}}{2}, -x_\delta]$ and for $x \in [x_\delta, \frac{\mathcal{T}}{2}]$, for some asymptotically small $x_\delta > 0$, and

(iii) is near a homoclinic orbit of the unperturbed system,

$$\Gamma_m(\xi) = (u_m(\xi), v_m(\xi)) = (u_0, \frac{3b}{2u_0} \operatorname{sech}^2 \left(\frac{\sqrt{b}\xi}{2} \right)) + \mathcal{O}(\delta^{1-\beta}), \quad (2.8)$$

for $-\Xi < \xi < \Xi$, where

$$u_0 = u_0(m, a, b) = 3bm\sqrt{\frac{b}{a}} \quad \text{for } m > 1. \quad (2.9)$$

Remark 2.4. The fast segments (or singular v -pulses) of the periodic states given by Theorem 2 lie exponentially close to the transverse intersections of the stable and unstable manifolds of \mathcal{M} . In addition, the one-pulse homoclinic solutions described in section 2.1 can be interpreted as the infinite-period limit of the family of periodic solutions ($\lim_{m \downarrow 1} \mathcal{T}(m) = \infty$ (2.7)). Moreover, the boundary $m = 1$ of the above interval $m > 1$ corresponds precisely to the value of u_0 that the u -component of the one-pulse homoclinic solutions have in the fast regime.

Remark 2.5. Formula (2.7) for $\mathcal{T}(m)$ can be derived from equations (4.9) and (4.10) in [5]. In section 7 on the numerical simulations, we need to derive the value of m from an observed periodic pattern. This can be done by using an inverted version of (2.7) – see also (4.11) in [5]:

$$m(\mathcal{T}) = \frac{E(\mathcal{T})^2 + 1}{E(\mathcal{T})^2 - 1} \quad \text{where } E(\mathcal{T}) = e^{\frac{1}{2}\mathcal{T}\delta\sqrt{a}} \quad (2.10)$$

Remark 2.6. In [5], additional stationary solutions, such as multiple-pulse homoclinic solutions and various other types of spatially periodic patterns, have been constructed, also using the methods of geometric singular perturbation theory. However, since these solutions have not yet been observed in the numerical simulations, we do not pay attention to them in this paper.

3 The main stability results

In order to fix notation for the stability analysis, we denote the stationary solutions of (1.2) described in the previous section by

$$(u(x, t), v(x, t)) = (U_0(x; \beta, m, a, b), V_0(x; \beta, m, a, b)),$$

where, by rescaling (2.2), $(U_0(x), V_0(x))$ corresponds either to the one-pulse pattern $\Gamma_1(\xi)$ (Theorem 1, $m = 1$ (Remark 2.4)), or to a periodic pattern $\Gamma_m(\xi)$ (Theorem 2, $m > 1$). In order to apply a linear stability analysis, we look at solutions of the full partial differential equation that lie nearby:

$$(u(x, t), v(x, t)) = (U_0(x), V_0(x)) + \epsilon e^{\lambda t}(U(x), V(x)) + \mathcal{O}(\epsilon^2). \quad (3.1)$$

Plugging this Ansatz into the full partial differential equation (1.2) and neglecting terms of $\mathcal{O}(\epsilon^2)$, the linearized stability of the stationary pattern (u_0, v_0) with respect to perturbations is determined by the following singularly perturbed eigenvalue problem:

$$\begin{aligned} \lambda U &= \frac{d^2 U}{dx^2} - V_0^2 U - 2U_0 V_0 V - \delta^2 a U \\ \lambda V &= \delta^2 \frac{d^2 V}{dx^2} + V_0^2 U + 2U_0 V_0 V - b\delta^\beta V, \end{aligned} \quad (3.2)$$

with the ‘boundary condition’ that U and V remain bounded as $x \rightarrow \pm\infty$.

The continuous spectrum of the solutions is located in the left half plane. It is the set of λ such that $\lambda < -A$, $-B < 0$ (for any $0 < \delta \ll 1$). Thus, the continuous spectrum will not play a role in the asymptotic stability analysis. However, the continuous spectrum does approach $\lambda = 0$ in the limit $\delta \rightarrow 0$, therefore one has to take the continuous spectrum into account if one wants to prove the stability of the singular homoclinic pattern by an Evans function approach, see [6] for all details.

The main analytical results obtained in this paper are as follows. They hold for each $\mathcal{O}(1)$ value of a . First, if $0 \leq \beta < 1/2$, then for all $\mathcal{O}(1)$ values of b , there are two positive eigenvalues $\lambda \mathcal{O}(\delta^{1-\beta})$ and $\frac{5}{4}b\delta^\beta$ whose associated eigenfunctions are bounded solutions of (3.2); and hence formally, both the one-pulse and the spatially-periodic stationary solutions (U_0, V_0) are always unstable for $B \gg \sqrt{\delta}$. Second, if $1/2 < \beta < 1$, then for no $\mathcal{O}(1)$ value of the parameter b does there exist an eigenvalue λ with positive real part for which (3.2) has bounded eigenfunctions; hence formally it appears that the underlying one-pulse and spatially-periodic stationary solutions (U_0, V_0) are stable for $\delta \ll B \ll \sqrt{\delta}$. Third, the case when $\beta = 1/2$ is a transition case between the above two regimes. When $\beta = 1/2$, there exists a critical value $b_H = b_H(a, m)$, often abbreviated to $b_H(m)$, of b at which a subcritical Hopf bifurcation occurs. For $b > b_H(m)$ there exists a pair of eigenvalues with positive real parts, which lie near 0 and $\frac{5}{4}b\delta^\beta$ respectively, for very large b , then merge at a value labeled $b_c(m)$ into a complex conjugate pair as b decreases, and finally as b decrease toward $b_H(m)$ this pair migrates to the imaginary axis. For $b > b_H(m)$ the stationary

patterns $(U_0(x; 1/2, m, a, b), V_0(x; 1/2, m, a, b))$ are linearly unstable, while for $b < b_H(m)$ they are formally stable. We note, for example, that $b_H \approx 0.66$ when $a = 1.0$ and $m = 1$, and that $b_H(m)$ is a decreasing function of m , see (5.16). Fourth, there exists a critical value of $B_D(m) = \delta b_D(m)$ for some $\mathcal{O}(1)$ value of $b_D(m)$ at which the stationary solutions disappear. For each m , this critical value lies on the right edge of the interval of β values, namely $[0, 1)$, for which the existence results of [5] apply, and there is no longer a sharp distinction between fast and slow variables.

Remark 3.1. The spectrum of a periodic wave generally consists of loops or bands of eigenvalues, rather than discrete points (see e.g [11]). For large wavelength periodic waves which are close to a homoclinic limit with a simple isolated eigenvalue λ_0 , it is known that periodic waves of sufficiently large wavelength will have a loop spectrum in a small neighborhood of λ_0 [12]. In the event that $\text{Re} \lambda_0 > 0$, this is sufficient to obtain a rigorous proof of instability of the large wavelength periodic waves. However, when the homoclinic limit is stable and $\lambda_0 = 0$, no conclusion can yet be drawn for the periodic wave. The periodic waves Γ_m and their limiting homoclinic wave in the one-dimensional Gray-Scott model satisfy the hypotheses of Theorem 1.2 in [12]. Hence we may conclude that in the parameter regime where Γ_1 is linearly unstable, that Γ_m is as well, for m sufficiently close to 1.

Remark 3.2. Regarding the notation convention, we use the same set of variables u, p, v, q (and their capitalized versions) for both the underlying stationary solution and the components of the solution of the eigenvalue problem. No confusion arises, however, since the subscript zero is used to indicate that the variable in question denotes a component of the wave solution itself. Moreover, we shall use lower case variables to denote the slow segments of the eigenfunctions (functions of the slow/outer variable x) and capital letters to denote the fast segments (functions of the fast/inner variable ξ).

The first three main analytical results will be established in section 5, and section 6 is devoted to the fourth result. As preparation, in section 4, we identify the significant scalings of the eigenvalue and eigenfunctions in (3.2), and we explicitly reduce the scaled fourth-order eigenvalue problem to a nonlocal second-order equation.

We will search for eigenvalue-bounded eigenfunction pairs of the scaled eigenvalue problem with $\text{Re}(\lambda) > 0$. By examining the slow and fast regimes of (3.2), we will find that u must be constant ($\delta^\alpha \hat{c}$ to leading order) during the excursion of v_0 through the fast field, just as u_0 is constant there. The value of \hat{c} is determined by matching the jump discontinuity in the value of the first derivative of u that occurs during a pulse in v_0 to the behavior of u in the slow field (see Figure 3). More importantly, the value of \hat{c} is critical for determining how strongly the slow and fast regimes of (3.2) are coupled.

For example, we will show that $\hat{c} \ll 1$ when $\beta < 1/2$, see section 4.1 for the introduction of \hat{c} and formula (4.12) for its explicit determination. Hence, to leading order, (3.2) will reduce to the standard uncoupled eigenvalue equation:

$$\lambda v = \delta^2 \frac{d^2 v}{dx^2} + 2u_0 v_0 v - b\delta^\beta v;$$

and this equation is precisely the eigenvalue problem arising from the stationary homoclinic solution of the uncoupled Fisher-KPP equation

$$V_t = \delta^2 V_{xx} + U_0 V^2 - b\delta^\beta V.$$

In particular, by (2.2) and $\hat{t} = \delta^\beta t$, the F-KPP equation may be written as:

$$\hat{V}_{\hat{t}} = \hat{V}_{\hat{x}\hat{x}} + \hat{U}_0 \hat{V}^2 - b \hat{V}, \quad (3.3)$$

which clearly has one $\mathcal{O}(1)$ unstable eigenvalue (see section 5). Therefore, we will be able to formally conclude that there is always an unstable eigenvalue $\lambda > 0$ of $\mathcal{O}(\delta^\beta)$ if $\beta < \frac{1}{2}$.

By contrast, when $\beta \geq 1/2$, one cannot neglect the coupling between the fast field and the slow field, since $\hat{c} = \mathcal{O}(1)$ in that case. In these regimes, the location of the eigenvalues is determined by the full nonlocal eigenvalue problem (NLEP) for v derived in section 4 and studied in section 5.

4 Reduction of the singularly perturbed eigenvalue problem to a nonlocal eigenvalue problem

In this section, we show that (3.2) reduces to a scalar, though nonlocal, eigenvalue problem. We begin by analyzing (3.2) separately in the fast and slow regimes. That the solutions $(U(x), V(x))$ of (3.2) must have fast and slow segments over precisely the same x -intervals (ξ -intervals) as (U_0, V_0) does can already be determined directly from (3.2). During slow intervals in which V_0 is exponentially small (*i.e.*, outside of the $\mathcal{O}(\delta^{1-\frac{1}{2}\beta})$ narrow x -interval(s) during which V_0 makes a fast jump and inside of which dU_0/dx has a jump discontinuity), the equation for U can be written as

$$\frac{d^2 U}{dx^2} - (\lambda + \delta^2 a)U = \text{exp. small.}$$

Now, for definiteness, we suppose that there is a jump discontinuity in dU_0/dx at $x = 0$. If the U component of the solution $(U(x), V(x))$ is continuous at $x = 0$ and if its derivative is also continuous there (*i.e.*, if there is no jump discontinuity in dU/dx), then when λ has positive real part it follows from the above equation that the solutions U must become unbounded as $x \rightarrow \infty$ and/or $\rightarrow -\infty$. Hence, in order for a bounded eigenfunction to exist, we conclude that the destabilizing perturbations (U, V) must, at minimum, have a jump discontinuity in dU/dx at $x = 0$, and also at each of the other points where dU_0/dx does. To see that there are no further jump discontinuities, we observe that, when λ has positive real part, the V equation has only exponentially growing solutions (*i.e.*, unbounded as $x \rightarrow \pm\infty$) in the regions where V_0 is exponentially small, and these cannot be matched.

4.1 The fast system

During the fast V -jump, we need to substitute the scalings (2.2) of the stationary pattern (U_0, V_0) into (3.2). We also scale λ , U , and V , since there is no reason to expect that these quantities have to remain $\mathcal{O}(1)$. A complete scaling analysis is performed in Appendix A: first, we introduce $\lambda = \delta^\ell b \hat{\lambda}$, $U = \delta^{\frac{3}{2}\beta} u$, and $V = \delta^{-\frac{1}{2}\beta} v$ for any $\ell \in \mathbf{R}$ (where the b in the scaling for λ has been introduced for convenience and it is always assumed to be $\mathcal{O}(1)$); and then we find that the main significant scaling such that unstable eigenvalues might exist is: $\ell = \beta$. Indeed, the scaling of λ is corroborated by the above formal argument. As discussed in the appendix, the scaling of U and V may be taken to be the same as that of U_0 and V_0 (2.2). Hence, we take:

$$\lambda = \delta^\beta b \hat{\lambda}, U = \delta^{\frac{3}{2}\beta} u, V = \delta^{-\beta/2} v. \quad (4.1)$$

By this scaling we know that $\hat{\lambda}$ is always $\mathcal{O}(1)$, while u and v are $\mathcal{O}(1)$ during the fast segments. Inserting (2.2) and (4.1) into (3.2) yields:

$$\begin{aligned} u_{\xi\xi} - \delta^{2(1-\beta)} \left(v_0^2 + \delta^{2\beta} b \hat{\lambda} + \delta^{2+\beta} a \right) u &= 2\delta^{2(1-\beta)} u_0 v_0 v \\ v_{\xi\xi} + \left(2u_0 v_0 - b - b \hat{\lambda} \right) v &= -v_0^2 u, \end{aligned} \quad (4.2)$$

where the subscript ξ denotes the total derivative with respect to ξ . Recall that u_0 and v_0 are given in (2.3) and (2.5).

Now, one observes straightaway that, in (4.2), u is constant to leading order during the interval in which a pulse occurs, since $0 \leq \beta < 1$ implies that all of the terms in (4.2)(a), except $u_{\xi\xi}$, are $\ll 1$. Hence, we write $u = \hat{c} + \text{h.o.t}$ during an excursion through the fast field, and to leading order (4.2)(b) simplifies to the following scalar eigenvalue problem:

$$v_{\xi\xi} + \left(2u_0 v_0 - b - b \hat{\lambda} \right) v = -\hat{c} v_0^2. \quad (4.3)$$

Although u remains constant (to leading order), we can compute the jump discontinuity $\Delta_f u_\xi$ in u_ξ during the fast excursion using (4.2(a)). The exact expression for this jump discontinuity is given by:

$$\Delta_f u_\xi = \int_{\xi_0 - \frac{T_f}{2}}^{\xi_0 + \frac{T_f}{2}} u_{\xi\xi} d\xi,$$

where T_f is the time the steady solution about which we have linearized takes to return to a fixed neighborhood of the slow manifold \mathcal{M} . For example, if the size of this neighborhood is $\mathcal{O}(1)$, then $T_f = \mathcal{O}(1)$. In the case we are interested in, however, the size of the neighborhood is $\ll 1$; we take $T_f = \mathcal{O}(1/\sqrt{\delta})$. Also, here ξ_0 denotes the time at which the maximum of the V_0 -pulse occurs, and without loss of generality the parametrization is chosen so that $\xi_0 = 0$.

Now, asymptotically as $\delta \rightarrow 0^+$, this jump discontinuity is given to leading order by:

$$\Delta_f u_\xi = \delta^{2(1-\beta)} \int_{-\infty}^{\infty} \left[\hat{c} v_0^2 + 2u_0 v_0 v \right] d\xi + \text{h.o.t.} \quad (4.4)$$

This may be seen as follows. First, the leading order terms in the u equation are those involving v_0 , which are of $\mathcal{O}(\delta^{2(1-\beta)})$. Next, due to the exponential contraction of v_0 to zero as $\xi \rightarrow \pm\infty$, one sees directly that the integrals of these terms from $\xi_0 + T_f/2$ to ∞ and from $-\infty$ to $\xi_0 - T_f/2$ are exponentially small. Hence, for these two terms, the domain of integration may be extended to the entire real line without altering their leading order asymptotic behavior. Finally, for the other two terms in the u equation, integration over the interval of length $\mathcal{O}(1/\sqrt{\delta})$ shows that they remain of higher order. We also recall that $u = \mathcal{O}(1)$ is assumed. Therefore, (4.4) gives the correct leading order asymptotic behavior for $\Delta_f u_\xi$.

Remark 4.1. So far, there is no difference between the $m = 1$ and $m > 1$ cases.

4.2 The slow system

In this subsection, we analyze (3.2) while U_0 and V_0 are in the slow regime. We consider the U and V variables during the slow segments on either side of a fast excursion and denote these solutions by U_ℓ, V_ℓ and U_r, V_r , respectively.

During the x intervals corresponding to the slow regimes of the stationary solutions, we know that $V_0(x; \beta, m, a, b)$ is exponentially small. Hence, in these regimes, the full eigenvalue problem (3.2) simplifies considerably to:

$$\begin{aligned} U_{xx} - (\delta^\beta b \hat{\lambda} + \delta^2 a) U &= \text{exp. small} \\ \delta^2 V_{xx} - b \delta^\beta (1 + \hat{\lambda}) V &= \text{exp. small.} \end{aligned} \quad (4.5)$$

Here, we use the outer (slow) x variable again, the subscript x denotes the total derivative on x , and we have returned to the unscaled variables, although we have retained the scaling of λ as $\delta^\beta b \hat{\lambda}$.

Since we look for unstable eigenvalues, the simplified equation (4.5) directly yields the form of the two slow segments of the eigenfunction U , one on either side of the fast excursion (which is at $x = 0$ without loss of generality):

$$\begin{aligned} U_\ell &= c_\ell^+ e^{\delta^{\frac{\beta}{2}} \sqrt{b \hat{\lambda}} x} + c_\ell^- e^{-\delta^{\frac{\beta}{2}} \sqrt{b \hat{\lambda}} x} + \text{h.o.t} \quad \text{for } x < 0 \\ U_r &= c_r^+ e^{\delta^{\frac{\beta}{2}} \sqrt{b \hat{\lambda}} x} + c_r^- e^{-\delta^{\frac{\beta}{2}} \sqrt{b \hat{\lambda}} x} + \text{h.o.t} \quad \text{for } x > 0. \end{aligned}$$

To determine the four unknown coefficients, we treat the cases $m = 1$, corresponding to the one-pulse solutions and $m > 1$, corresponding to the periodic solutions, separately.

When $m = 1$, the eigenfunctions (and in particular their U components) must remain in the slow field for all $x < 0$ and for all $x > 0$, because these semi-infinite time intervals are the slow regimes for the stationary solutions ($U_0(x), V_0(x)$). Hence, we must require $c_\ell^- = c_r^+ = 0$ so that U_ℓ and U_r stay bounded as $x \rightarrow \mp\infty$, respectively. In addition, since U is constant to leading order during the excursion in the fast field and since $U(x)$ is a continuous function, we must impose the matching condition:

$$\lim_{x \rightarrow 0^-} U_\ell(x) = \lim_{x \rightarrow 0^+} U_r(x). \quad (4.6)$$

Therefore, when $m = 1$, we have to leading order:

$$\begin{aligned} U_\ell &= c_\ell^+ e^{\delta^{\frac{\beta}{2}} \sqrt{b \hat{\lambda}} x} \quad \text{for } x < 0 \\ U_r &= c_\ell^+ e^{-\delta^{\frac{\beta}{2}} \sqrt{b \hat{\lambda}} x} \quad \text{for } x > 0. \end{aligned} \quad (4.7)$$

When $m > 1$, the stationary solutions ($U_0(x), V_0(x)$) of (3.2) remain in the slow field only for $|x| \leq \mathcal{O}(\frac{1}{\delta})$, see equation (2.6) in section 2, instead of for all $|x| \neq 0$ as was the case above for $m = 1$. Hence, we may only require that U stays bounded for $|x| = \mathcal{O}(\frac{1}{\delta})$. Working on $x < 0$, we find for $x = -\frac{1}{\delta}$ that, $U_\ell = [\text{exp. small} + c_\ell^- e^{\sqrt{b \hat{\lambda}} \delta^{\frac{\beta}{2}} - 1}]$. This value grows without bound as $\delta \rightarrow 0^+$ for all $\beta \in [0, 1)$ unless c_ℓ^- is chosen to be exponentially small. Hence, for $m > 1$, we require $c_\ell^-, c_r^+ = \text{exp. small}$. Moreover, by imposing the same matching condition (4.6) as employed when $m = 1$, the outer solutions are also (4.7) to leading order for $m > 1$.

Next, the magnitude of c_ℓ^+ , the only remaining unknown coefficient, is determined by matching the values of u in the fast and slow regimes. Recalling from subsection 4.1 that $u = \hat{c}$ to leading order during the fast excursion, and recalling the scaling (4.1) of u introduced there, we match and obtain:

$$c_\ell^+ = \delta^{\frac{3}{2}\beta} \hat{c}. \quad (4.8)$$

Thus, c_ℓ^+ has now been expressed in terms of \hat{c} , the only unknown constant left in the eigenvalue equation for the fast field. In subsection 4.1, we computed the jump discontinuity in u_ξ , $\Delta_f u_\xi$ (4.4). This quantity should match the jump discontinuity, $\Delta_s U_x$, in the x -derivative of the slow parts of the solutions, $U_\ell(x)$ and $U_r(x)$ (see Figure 3). Since we know (4.7) and (4.8) hold for all $m \geq 1$, we directly compute:

$$\Delta_s U_x = \lim_{x \rightarrow 0^+} \frac{dU_r}{dx}(x) - \lim_{x \rightarrow 0^-} \frac{dU_\ell}{dx}(x) = -2\delta^{2\beta} \sqrt{b\hat{\lambda}} \hat{c}. \quad (4.9)$$

Remark 4.2. We will find in section 5 that $v(\xi)$ decreases exponentially fast to 0 as $|\xi| \rightarrow \infty$. Thus, just like $V_0(x)$, $V(x)$ is exponentially small in the slow regime; and this justifies our relying exclusively on (4.5(a)) in this subsection, while ignoring (4.5(b)).

4.3 Determination of \hat{c}

In this subsection, we determine \hat{c} by matching the jump discontinuities, $\Delta_f u_\xi$ and $\Delta_s U_x$, in the derivatives of the first component as calculated in the previous two subsections.

As a preliminary step, we express $\Delta_s U_x$ as it is given by (4.9) in terms of the scaled variables used in subsection 4.1, namely $x = \delta^{1-\frac{\beta}{2}} \xi$ (recall (2.2)) and $U = \delta^{\frac{3}{2}\beta} u$,

$$\Delta_s u_\xi = -2\delta \hat{c} \sqrt{b\hat{\lambda}}. \quad (4.10)$$

Hence, equating this value of the jump discontinuity with that given in (4.4) of subsection 4.2, and cancelling out one factor of δ from both sides, we obtain:

$$-2\sqrt{b\hat{\lambda}} \hat{c} = \delta^{1-2\beta} \left[\hat{c} \int_{-\infty}^{\infty} v_0^2(\xi) d\xi + 2u_0 \int_{-\infty}^{\infty} v_0(\xi) v(\xi) d\xi \right]. \quad (4.11)$$

Next, we compute to leading order:

$$\int_{-\infty}^{\infty} v_0^2(\xi) d\xi = \frac{6b\sqrt{b}}{u_0^2},$$

where we used the explicit expression (2.4), see also [5]. Plugging this into the above equation and solving for \hat{c} yields:

$$\hat{c} = \frac{-\delta^{1-2\beta} u_0^3}{3b\sqrt{b}\delta^{1-2\beta} + u_0^2\sqrt{b\hat{\lambda}}} \int_{-\infty}^{\infty} v_0(\xi) v(\xi) d\xi. \quad (4.12)$$

Note that this result yields the critical value $\frac{1}{2}$ for β :

$$\begin{aligned} 0 \leq \beta < \frac{1}{2} &\rightarrow |\hat{c}| = \mathcal{O}(\delta^{1-2\beta}) \ll 1 \\ \frac{1}{2} \leq \beta < 1 &\rightarrow |\hat{c}| = \mathcal{O}(1) \end{aligned}$$

Moreover, \hat{c} simplifies considerably if $\beta > \frac{1}{2}$:

$$\hat{c} = -\frac{u_0^3}{3b\sqrt{b}} \int_{-\infty}^{\infty} v_0(\xi) v(\xi) d\xi + \mathcal{O}(\delta^{2\beta-1}). \quad (4.13)$$

Substituting the general expression (4.12) for \hat{c} into (4.3), we obtain to leading order a reformulation of the singularly perturbed eigenvalue problem (3.2) as the following nonlocal eigenvalue problem (NLEP):

$$v_{\xi\xi} + \left(2u_0v_0(\xi) - b - b\hat{\lambda}\right)v = \frac{\delta^{1-2\beta}u_0^3v_0^2(\xi)}{3b\sqrt{b}\delta^{1-2\beta} + u_0^2\sqrt{b\hat{\lambda}}} \int_{-\infty}^{\infty} v_0(\xi)v(\xi)d\xi. \quad (4.14)$$

To leading order, the difference between the stability problem for the homoclinic pattern and that for the periodic patterns is represented by the value of m that appears only implicitly in the NLEP through $u_0 = u_0(m, a, b)$, see formulae (2.3) and (2.9).

Remark 4.3. For $\beta < \frac{1}{2}$, (4.14) reduces, to leading order, to the linearized eigenvalue problem around the stationary homoclinic solution of the uncoupled Fisher-KPP equation (3.3). As discussed in section 3, this solution is unstable, and thus we know that there exists a positive $\mathcal{O}(1)$ eigenvalue when $\beta < \frac{1}{2}$. This eigenvalue shall be recovered in the next section when we study (4.14) with $\sigma = \delta^{1-2\beta}$ as a parameter.

Remark 4.4. The presence of the term $\sqrt{\hat{\lambda}}$ in NLEP (4.14) is a notable difference between the full eigenvalue problem and the NLEP. In [6], we show that the NLEP equation has an associated Evans function with a $1/\sqrt{\hat{\lambda}}$ singularity at the origin. This branch point necessitates the continuation of the Evans function to a two-sheeted Riemann surface \mathcal{R} . The branch point contributes a singularity of *fractional* order to this Evans function, so that its winding number relative to a curve on \mathcal{R} containing the origin in its interior is -1 . This is used in the index calculation for the perturbed wave to obtain a rigorous proof that the only small eigenvalue is the translational eigenvalue at $\hat{\lambda} = 0$, and that this eigenvalue is simple.

Remark 4.5. The NLEP can be made into a local problem by introducing two new variables $R(\xi) \equiv \int_{-\infty}^{\xi} v_0(s)v(s)ds$ and $S(\xi) \equiv \int_{\xi}^{\infty} v_0(s)v(s)ds$, so that the integral on the right hand side of the NLEP is simply $R + S$, and then by appending the two equations $R_{\xi} = v_0v$ and $S_{\xi} = -v_0v$. But, this approach is not needed here.

5 The nonlocal eigenvalue problem

In this section, we explicitly determine the parameter regimes in which (4.14) has positive eigenvalues whose associated eigenfunctions are bounded as $x \rightarrow \pm\infty$ and those regimes in which no such eigenvalue-eigenfunction combinations exist. In particular, for all combinations of the positive parameters a, m , and σ , we determine the number and location of eigenvalues with positive real part for each of value of the parameter b . The work relies heavily on the theory of hypergeometric functions.

5.1 Explicit eigenvalue formulae

Let $t = \frac{1}{2}\sqrt{b}\xi$, $y(t) = v(\xi)$, and $\sigma = \delta^{1-2\beta}$. Also, define new parameters:

$$P^2 = 4(1 + \hat{\lambda}) \quad \text{and} \quad C = \frac{9}{1 + 3\frac{b^2m^2}{a\sigma}\sqrt{\hat{\lambda}}}. \quad (5.1)$$

In these new variables and parameters, the NLEP (4.14) becomes ((2.3), (2.4), (2.8), (2.9)):

$$\ddot{y} + \left(\frac{12}{\cosh^2 t} - P^2 \right) y = \frac{C}{\cosh^4 t} \int_{-\infty}^{\infty} \frac{y(t)}{\cosh^2 t} dt, \quad (5.2)$$

with the boundary condition that $y : \mathbf{R} \rightarrow \mathbf{C}$ remains bounded as $t \rightarrow \pm\infty$.

The unique solution of this nonlocal eigenvalue problem is determined as follows. First, one transforms – in standard fashion (see for instance [24]) – the left hand side into the form of a hypergeometric differential equation by setting $y(t) = F(t)/(\cosh t)^P$ and then changing independent variables to $x \equiv \frac{1}{2}(1 - \tanh t)$:

$$x(1-x)F'' + (1+P)(1-2x)F' + (12-P-P^2)F = 2C(4x(1-x))^{1-\frac{P}{2}} \int_0^1 (4x(1-x))^{\frac{P}{2}} F(x) dx. \quad (5.3)$$

Second, one finds the unique solution $F_{\tilde{C}}$ of the auxiliary (standard, inhomogeneous) problem:

$$x(1-x)F_{\tilde{C}}'' + (1+p)(1-2x)F_{\tilde{C}}' + (12-P-P^2)F_{\tilde{C}} = \tilde{C}(4x(1-x))^{1-\frac{P}{2}} \quad (5.4)$$

where \tilde{C} is a constant. Recall that $F(a, b|c|z)$ and $z^{1-c}F(b-c+1, a-c+1|2-c|z)$ are two linearly independent solutions of the hypergeometric differential equation

$$z(1-z)F'' + [c - (a+b+1)z]F' - abF = 0.$$

From (5.4), one sees directly that $a = P + 4$, $b = P - 3$, and $c = P + 1$ (where a and b are interchangeable, and where of course there should be no confusion from briefly abusing these three letters in these few lines), and hence the two homogeneous solutions are:

$$\begin{aligned} X(x) &= F(P+4, P-3|P+1|x) \\ Y(x) &= \frac{L(P)}{x^P} F(-3, 4|1-P|x), \end{aligned} \quad (5.5)$$

where $L(P) \equiv \frac{(P-3)(P-2)(P-1)}{(P+3)(P+2)(P+1)}$. By the introduction of this additional constant we have $X(1-x) = Y(x)$ (which will be used frequently below). By solving the (standard) differential equation for the Wronskian $W(x)$, we find

$$W(x) \equiv XY' - YX' = \frac{w(P)}{(4x(1-x))^{1+P}}, \quad (5.6)$$

where $w(P) = -4^{1+P}PL(P)$. Moreover, we note that $X(x)$ is analytic at $x = 0$, and that $F(-3, 4|1-P|x)$ is a cubic polynomial. Now, the solution of the inhomogeneous problem is obtained via variation of constants; i.e., by setting $F_{\tilde{C}}(x) = f(x)X(x) + g(x)Y(x)$. Using (5.6), we find

$$\begin{aligned} f' &= \frac{4^{1-\frac{P}{2}}\tilde{C}}{P(P-1)(P-2)(P-3)}(1-x)^{1+\frac{P}{2}}x^{1-\frac{P}{2}}K(P, x) \\ g' &= -\frac{4^{1-\frac{P}{2}}\tilde{C}}{P(P-1)(P-2)(P-3)}x^{1+\frac{P}{2}}(1-x)^{1-\frac{P}{2}}K(P, 1-x), \end{aligned} \quad (5.7)$$

where the cubic polynomial $K(P, \xi) \equiv k_0(P) + k_1(P)\xi + k_2(P)\xi^2 + k_3(P)\xi^3$ with $k_0(P) = (P - 3)(P - 2)(P - 1)$, $k_1(P) = 12(P - 3)(P - 2)$, $k_2(P) = 60(P - 3)$, and $k_3(P) = 12$ can be obtained from $F(-3, 4|1 - P|x)$. Therefore, defining

$$\mathcal{F}(x_1, x_2, P) = \int_{x_1}^{x_2} (1 - \xi)^{1+\frac{P}{2}} \xi^{1-\frac{P}{2}} k(P, \xi) d\xi, \quad (5.8)$$

the general solution of the inhomogeneous equation (5.3) is:

$$F_{\tilde{C}}(x; P) = [d(P)\mathcal{F}(0, x; P) + f_0]Y(1 - x; P) + [-d(P)\mathcal{F}(1 - x, 1; P) + g_0]Y(x; P), \quad (5.9)$$

where $d(P) \equiv \frac{4^{1-\frac{P}{2}}\tilde{C}}{P(P-1)(P-2)(P-3)}$ (and of course \tilde{C} is a function of P) and f_0 and g_0 are constants determined by boundary conditions. Specifically, requiring that $F_{\tilde{C}}$ stay bounded as $x \rightarrow 0$ and as $x \rightarrow 1$ implies $g_0 = 0$ (since $Y(x) \rightarrow \infty$ as $x \rightarrow 0^+$ and $\mathcal{F}(1, 1; P) = 0$), while $f_0 = -d(P)\mathcal{F}(0, 1; P)$ (since $Y(1 - x) \rightarrow \infty$ as $x \rightarrow 1^-$ and $\mathcal{F}(0, 1; P) \neq 0$). We also observe that $F_{\tilde{C}}(1 - x; P) = F_{\tilde{C}}(x; P)$; and, for completeness, we record that

$$\mathcal{F}(0, 1; P) = -\frac{1}{24}P^2\left(1 + \frac{1}{2}P\right)^2\left(1 - \frac{1}{2}P\right)^2 \frac{\pi}{\sin(\frac{\pi}{2}P)}.$$

Third, in order that the solution $F_{\tilde{C}}(x; P)$ given by (5.9) of the auxiliary problem solves the full nonlocal problem (5.3), one requires that $F_{\tilde{C}}$ satisfies the consistency condition:

$$\tilde{C} = 2C \int_0^1 F_{\tilde{C}}(x; P) (4x(1 - x))^{\frac{P}{2}} dx. \quad (5.10)$$

Of course, due to the linearity of the auxiliary equation, its unique solution is of the form $F_{\tilde{C}}(x; P) = \tilde{C}F_1(x; P)$. Hence, for nonzero \tilde{C} , the consistency condition (5.10) simplifies to:

$$1 = 2C \int_0^1 F_1(x; P) (4x(1 - x))^{\frac{P}{2}} dx. \quad (5.11)$$

Finally, inserting the solution (5.9) into the relation (5.11), we obtain:

$$C(P) = \frac{P(P - 1)(P - 2)(P - 3)}{16\mathcal{R}(P)}, \quad (5.12)$$

where

$$\mathcal{R}(P) = -\int_0^1 \mathcal{F}(x, 1; P)Y(1 - x; P)x^{\frac{P}{2}}(1 - x)^{\frac{P}{2}} dx. \quad (5.13)$$

In Figure 4, the function $C(P)$ has been plotted for $P \geq 2$. We remark that a straightforward expansion yields:

$$\lim_{P \rightarrow 2} C(P) = \frac{9}{2} \quad (5.14)$$

Finally, the explicit expression (5.12) for $C = C(P)$ gets plugged into the the explicit expression for $b = b(P, C(P))$, which is readily obtained by inverting (5.1(b)):

$$b^2 = \frac{2a\sigma}{3m^2} \frac{1}{\sqrt{P^2 - 4}} \left[\frac{9}{C(P)} - 1 \right]. \quad (5.15)$$

This relation between b and P , and thus also the relation between b and $\hat{\lambda}$, determines the leading order part of the (discrete) eigenvalues of the NLEP. Using the explicit expressions (5.8), (5.12) and (5.13) one can explicitly solve (5.15). However, it is clear that this cannot be done by hand (especially not for complex values of P): Figures 4 and 5 have been obtained by using MATHEMATICA, [23].

The dependence of b on the parameters a, σ (i.e. β) and m only appears through the term $\frac{2a\sigma}{3m^2}$. This means that one only has to solve (5.15) for one set of the parameter values a, σ and m , for instance, $a = \sigma = m = 1$. Therefore, we now have in hand the most important outcome of solving (5.15): the critical value $b_H = b_H(a, \sigma, m)$ of b at which $\text{Re}(\hat{\lambda}) = 0$:

$$b_H(a, \sigma, m) = \frac{\sqrt{a\sigma}}{m} b_H(1, 1, 1) \approx \frac{\sqrt{a\sigma}}{m} 0.66 \quad \text{for } \hat{\lambda} \approx \pm 0.53i. \quad (5.16)$$

Remark 5.1. In section 7, we numerically check this behavior: (5.15) predicts that $\frac{b(a)}{\sqrt{a}}$, respectively $mb(m)$, should remain constant when a , respectively m , is varied.

Remark 5.2. The constant $\lambda = 0$ is always an eigenvalue, corresponding to translations, of the full eigenvalue problem (3.2) (see also (4.2)). Now, if we scratch the surface of the NLEP (4.14) (or equivalently (5.2)) a little bit, we recover the eigenvalue $\lambda = 0$. In fact, the derivative $dv_0/d\xi$ (or equivalently \dot{y}_0) of the stationary one-pulse solution Γ_1 is the eigenfunction associated to $\lambda = 0$. Then, from formula (2.4) for v_0 we see immediately that this derivative is an odd function of ξ (or of t). Hence, the integrals on the right hand sides of (4.14) and (5.2) vanish identically, and the second-order NLEP becomes a homogeneous equation for which it is known that $\lambda = 0$ is an eigenvalue, see also Remark 4.3. This also explains the restriction that \tilde{C} be nonzero as stated below formula (5.10), since $\tilde{C} = 0$ is the solution of (5.10) for this eigenvalue-eigenfunction pair.

Remark 5.3. As P approaches both endpoints of the interval $(2, 3)$, b^2 diverges to ∞ . It diverges as $P \rightarrow 2^+$ because the square root term in the denominator vanishes; whereas, it diverges as $P \rightarrow 3^-$ because then $C(P) \rightarrow 0$. Note that $\hat{\lambda} \rightarrow 0^+$ as $P \rightarrow 2^+$: these small (positive) eigenvalues correspond to those found in the Appendix in the scaling $\lambda = \delta^{1-\beta} b \tilde{\lambda}$, $0 \leq \beta \leq \frac{1}{2}$.

5.2 Hopf bifurcations

The explicit formulae (5.12) and (5.15) yield the eigenvalues. For each set of parameters a, m , and σ , if one is given a value of b , say b_0 , then the points of intersection of the horizontal line $b = b_0$ with the curve given by (5.12) and (5.15) are precisely the eigenvalues. Moreover, those pairs $(\text{Re}\hat{\lambda}, b)$ that lie off of the curve given by (5.12) and (5.15) do not correspond to eigenvalue-parameter pairs for which the eigenvalues have positive real parts.

Recalling $\sigma \equiv \delta^{1-2\beta}$, there are three cases, which are analyzed below (out of order):

Case I	$0 \leq \beta < \frac{1}{2}$	$\sigma \ll 1$	$\frac{2a\sigma}{3m^2} \ll 1$
Case II	$\beta = \frac{1}{2}$	$\sigma = 1$	$\frac{2a\sigma}{3m^2} = \mathcal{O}(1)$
Case III	$\frac{1}{2} < \beta < 1$	$\sigma \gg 1$	$\frac{2a\sigma}{3m^2} \gg 1$

Case I. The bottom curve $b = b(\text{Re}(\hat{\lambda}), a, m)$ shown in Figure 5 is obtained in case I. It lies close to the vertical lines $\text{Re}(\hat{\lambda}) = 0$ and $\text{Re}(\hat{\lambda}) = 5/4$ with a segment that is close to the $\text{Re}(\hat{\lambda})$ -axis. The “tail” emerging from the point marked $(\text{Re}(\hat{\lambda})_c, b_c)$, with $b_c \ll 1$, bends sharply to the left and crosses the b -axis with intercept $\ll 1$. Therefore, for each $\mathcal{O}(1)$ value of b , the horizontal line $b = \text{constant}$ intersects the curve $b = b(\text{Re}(\hat{\lambda}))$ in two points, each of which yields an unstable eigenvalue. The first one is very small and of the form $\lambda = b\hat{\lambda}\delta^\ell$ with $\ell = 1 - \beta$ and $\beta \geq 0$, see the discussion of region D_1 in Appendix A. By contrast, the second positive eigenvalue is $\hat{\lambda} \approx 5/4$, *i.e.*, $\lambda \approx \frac{5}{4}b\delta^\beta$. It is near the unstable eigenvalue of the stationary homoclinic solution of the rescaled one-dimensional Fisher-KPP equation (3.3). Hence, for all $\mathcal{O}(1)$ values of b , we have that Γ_m is unstable for all $m \geq 1$.

We remark that the subscript c on $b_c = b_c(a, m)$ has been introduced to indicate that the two distinct real eigenvalues that exist for $b > b_c$ merge there to become a complex conjugate pair for $b < b_c$. Also, just as the scaling of b_H with a is given by (5.16), we know that

$$b_c = b_c(a, \sigma, m) = \frac{\sqrt{a\sigma}}{m} b_c(1, 1, 1) \approx \frac{\sqrt{a\sigma}}{m} 0.99.$$

These results for Case I were not unexpected, since for $\beta < 1/2$ (*i.e.*, $\sigma < 1$), we have $C \ll 1$ and hence the right hand side of the NLEP (4.14) is a small perturbation of a well-known homogeneous equation. The one-pulse solutions are unstable in this case, because the coupling between the slow and fast fields is not sufficiently strong.

Case III. The top curve $b = b(\text{Re}(\hat{\lambda}), a, m)$ shown in Figure 5 is obtained in case III. It lies strictly in the regime $b \gg 1$, and thus $b_c \gg 1$ and $b_H \gg 1$. Hence, one sees straight away that, for each $\mathcal{O}(1)$ value of b , the horizontal lines $b = \text{constant}$ do not intersect the top curve, and there are no unstable eigenvalues. The stationary patterns Γ_m are formally stable in the regime $1 > \beta > \frac{1}{2}$ when the parameters a, b and m are $\mathcal{O}(1)$ and δ is sufficiently small.

Case II. The middle curve $b = b(\text{Re}(\hat{\lambda}), a, m)$ shown in Figure 5 is obtained in case II. For all $\mathcal{O}(1)$ values of a and m , the critical parameters b_H and b_c are $\mathcal{O}(1)$. Hence, for fixed a, m and δ , there are three distinguished intervals of $\mathcal{O}(1)$ b values:

For $b < b_H(a, m)$, there do not exist $\hat{\lambda}$ with positive real part;

For $b_H(a, m) < b < b_c(a, m)$, there exists a complex conjugate pair of eigenvalues $\hat{\lambda}$ with positive real part;

For $b_c(a, m) < b$, there exist two distinct, positive eigenvalues $\hat{\lambda}$.

In both the latter intervals, the stationary solutions Γ_m are unstable; however, at $b = b_H$, there is a Hopf bifurcation, and the stationary solutions Γ_m are stable for $b < b_H$. This bifurcation is illustrated in Figure 6, wherein the location of the eigenvalues is sketched as a function of b .

The leading order asymptotic behavior of $b_H(a)$ as a function of a can also be determined from the explicit formulae (5.12) and (5.15). We begin by recalling that, for $a = m = 1.0$, we have $\text{Re}(\hat{\lambda}) = 0$ when $b = b_H \approx 0.66$ (5.16). Therefore, because $\sigma = 1$, we get (at leading order):

$$b_H(a) \approx 0.66 \frac{\sqrt{a}}{m}. \quad (5.17)$$

From the formulae (5.12) and (5.15) and from Figure 5, one can determine how many of the solutions Γ_m are stable for a given value of b as follows. This determination is significant since there can be multiple stable periodic solutions, *i.e.*, for a given interval of length L (with homogeneous Neumann boundary conditions), several N -pulse patterns can coexist, for a given set of parameter values. Note that N , L and m are related by (2.10), see section 7.2 and Figures 1, 7 and 8.

Let $\mu \equiv \frac{\sqrt{a}}{m}$. With b fixed, there exists a critical curve, call it $\mu_* = \mu_*(b)$, such that $b_H(\mu_*) = b$; *i.e.*, the horizontal line of fixed b intersects the solution to (5.15) exactly at $\text{Re}(\hat{\lambda}) = 0$. We note that, if a and m conspire so that $\mu > \mu_*$, then the solution Γ_m with this same fixed b will be stable since the horizontal line does not intersect the curve given by (5.15). By contrast, if $\mu < \mu_*$, then there are either one or two such intersection points, *i.e.*, either two unstable complex valued eigenvalues, or two unstable real eigenvalues. In both cases the solution is unstable.

Moreover, we may define a critical value a_* of the parameter a by choosing $m = 1$:

$$a_* = a_*(b) = (\mu_*(b))^2. \quad (5.18)$$

The above analysis directly shows that, if $a < a_*(b)$, then $\mu < \mu_*$ and the solution Γ_m is unstable for this value of b . Instead, for $a > a_*(b)$, then $\mu > \mu_*$ for all $m \in [1, \sqrt{\frac{a}{a_*}}]$; *i.e.*, there exists an m -interval of stable patterns Γ_m . Note that this result is derived in the context of an unbounded x -domain. In section 7, we will perform simulations on bounded domains (mostly with homogeneous Neumann boundary conditions); hence, by (2.10), m can only attain certain discrete values. The above result indicates that for $a > a_*(b)$ several N -pulse patterns can be stable.

Remark 5.4. Case II may be thought of as the transition case, because it is precisely when b reaches an $\mathcal{O}(1)$ value of $b_H(a, m)$ that the coupling between the slow and the fast fields becomes strong enough to stabilize the singular pulse solutions Γ_m . Hence, this case represents the transition from case I, where the coupling is too weak ($b_H \ll 1$) and the solutions are unstable for all b of $\mathcal{O}(1)$, to case III, where the coupling is strong enough ($b_H \gg 1$) so that the singular patterns are stable for all b of $\mathcal{O}(1)$.

6 Disappearance of one-pulse homoclinic stationary states

In this section, we analyze the disappearance of the one-pulse homoclinic stationary states of (1.2). We will show that there is a critical value of the parameter $B = \delta^\beta b$ to be found in the scaling when $\beta = 1$ such that the one-pulse solutions exist for larger B (*i.e.*, for all b when $0 \leq \beta < 1$) but not for smaller B (*i.e.*, not for any b when $1 < \beta < 4$). Recalling section 2, we remark that the scaling $\beta = 1$ (*i.e.* $\alpha = 3/2$ in the notation of [5]) falls precisely on the open boundary of the interval $[0, 1)$ of β values for which the results of [5] apply. Hence, we use some different techniques, among them topological shooting, to study this phenomenon.

The analysis of this section is carried out on the following vector field:

$$\begin{aligned} \dot{u} &= \gamma p \\ \dot{p} &= \gamma \left(uv^2 - \delta^{2-\frac{1}{2}\beta} a + \delta^{2+\beta} a u \right) \\ \dot{v} &= q \\ \dot{q} &= -uv^2 + bv, \end{aligned} \quad (6.1)$$

with $\delta \ll 1$. This vector field is identical to (2.1) when $\gamma = \delta^{1-\beta}$ (and trivially $t \equiv \xi$ is the independent variable); and, when in addition $\gamma \ll 1$, (6.1) shares the same geometric features as (2.1). Also, for any $\gamma \in \mathbf{R}$, this vector field has the symmetry

$$t \rightarrow -t, p \rightarrow -p, q \rightarrow -q. \quad (6.2)$$

We remark that the γ here is not related to the scaled wave speed in [5].

We examine (6.1) in the following three regimes: $\gamma \ll 1$, $\gamma \gg 1$, and $\gamma = \mathcal{O}(1)$. Note that $\gamma = \mathcal{O}(1)$ corresponds to $B = b\delta^\beta = b\gamma\delta$, i.e. $B/\delta = b\gamma = \mathcal{O}(1)$ and $\beta = 1 - \frac{\log \gamma}{\log \delta}$. In the regime $\gamma \ll 1$, the analysis of section 4.1 in [5] may directly be used, and there it was shown that a unique stationary one-pulse homoclinic solution exists for each given pair (a, b) . In section 6.1, we briefly review the results needed from [5]. Then, in section 6.2, we show that, for $\gamma \gg 1$ (with the requirement that $\delta^{2-\frac{1}{2}\beta} \ll 1$) and for $\gamma = \mathcal{O}(1)$ but large, there do not exist one-pulse solutions for any $b \geq 0$. Finally, in section 6.3, we show that the result of section 6.1 can be extended to the regime in which $\gamma = \mathcal{O}(1)$ but γ is small. The analyses in sections 6.2 and 6.3 for $\gamma = \mathcal{O}(1)$ will suffice to show the desired results about the existence of a critical B in the scaling when $\beta = 1$ and the disappearance of one-pulse solutions. In section 7.2, we discuss the results of numerical simulations. These confirm that the B values at which the one-pulse solutions disappear lie in the $\beta = 1$ scaling.

Before launching into the analysis, we identify two important times at which the solutions under study have certain properties. Let $\Gamma^-(t) = (u^-(t), p^-(t), v^-(t), q^-(t))$ denote the solution of (6.1) on the unstable manifold of S that satisfies $v^-(t) > 0$ and that stays near the slow unstable manifold of S restricted to \mathcal{M} for a large interval of negative t values. Let \mathcal{B} be the neighborhood of the slow manifold \mathcal{M} defined by the set $\{(u, p, v, q) | \sqrt{v^2 + q^2} \leq \Delta; v, q \geq 0\}$. We denote by $t_0 < 0$ the time at which $\Gamma^-(t)$ first pierces the boundary of \mathcal{B} . Then, we define:

$$\begin{aligned} t_1 &\equiv \min_{t > t_0} \{q^-(t) = 0\} \\ t_2 &\equiv \min_{t > t_0} \{p^-(t) = 0\}. \end{aligned} \quad (6.3)$$

These two values, which may be finite or infinite, correspond to the times at which the q and p components, respectively, first vanish along a solution $\Gamma^-(t)$. They derive their importance from the symmetry (6.2), and in each of the three regimes for γ , we are interested in the relative order they occur, *i.e.*, whether $t_2 < t_1$, $t_2 > t_1$, or $t_2 = t_1$.

6.1 Asymptotically small γ ($\beta < 1$)

In this section, we explicitly take $\gamma \ll 1$ in (6.1). With this scaling, the system (2.1) with $0 \leq \beta < 1$ is precisely of the form of (6.1). In [5], it was shown that t_1 is finite, and following [5], the choice of $t_1 = 0$ fixes a unique parametrization of the solutions $\Gamma^-(t)$, so that $q(0) = 0$ and $v(0) > 0$. (Of course, the choice of t_0 above can be made in a fashion consistent with this parametrization.) Also, we use u_0^-, p_0^- to denote the values of the u and p coordinates of the solution $\Gamma^-(t)$ at time t_0 . We establish:

Proposition 6.1. Let $u_0 = u_0(m = 1, a, b)$ be as defined in (2.3)

$$\text{If } u_0^- \left\{ \begin{array}{l} = \\ < \\ > \end{array} \right\} u_0 + \text{h.o.t.}, \text{ then } t_2 \left\{ \begin{array}{l} = \\ < \\ > \end{array} \right\} t_1.$$

Proof of Proposition 6.1. As we have already stated, it follows from the proof of Theorem 4.1 in [5] that t_1 exists (and is set to 0) for all $u_0^- = \mathcal{O}(1)$. Moreover, during the fast, near-separatrix excursion, $u^-(t)$ stays constant to leading order equal to u_0^- , its value at t_0 . In other words, the solution $\Gamma^-(t)$ makes an excursion into the fast field staying close to the fast unstable manifold of the reduced fast system with $u \sim u_0^-$, and the q coordinate must vanish at $t_1 = 0$ due to this closeness result. Hence, we only need to compute $p_1 \equiv p^-(0)$ to prove the proposition.

It is clear that $p_1 = p_0^- + \int_{t_0}^0 \dot{p} dt$. Since $\dot{p} = \mathcal{O}(\gamma) \ll 1$, one can explicitly compute the leading order approximation of $\int_{t_0}^0 \dot{p} dt$ ($= \frac{1}{2}\Delta p$ in [5]) using the fact that the v and q components of orbits that leave the slow manifold \mathcal{M} through $(u_0^-, p_0^-, 0, 0)$ are $\mathcal{O}(\gamma)$ close to the homoclinic orbit of the unperturbed planar system $\ddot{v} = -u_0^- v^2 + bv$. Formula (3.18) in [5] directly yields: $\frac{1}{2}\Delta p = \gamma \frac{3b\sqrt{b}}{u_0^-} + \mathcal{O}(\gamma^3)$, where γ here plays the same role as ϵ in [5]. Due to the ‘doubly slow’ and linear character of the flow on \mathcal{M} (see Remarks 2.2 and 2.3), we find that $p_0^- = -\gamma\sqrt{a} + \text{h.o.t}$ (see section 6.3 and formula (3.7) in [5]). Putting these two formulae together yields:

$$p_1 = \gamma \left(-\sqrt{a} + \frac{3b\sqrt{b}}{u_0^-} \right) + \text{h.o.t.} \quad (6.4)$$

This last expression is the desired formula, since it explicitly gives p_1 as a function of u_0^- . It is identical to formula (4.2) in [5], see Theorem 4.1.

When u_0^- equals $u_0 \equiv 3b\sqrt{\frac{b}{a}} + \text{h.o.t}$, one finds $p_1 = 0$ to leading order, and hence, the orbit $\Gamma^-(t)$ is also forward asymptotic to S by the symmetry (6.2). Moreover, for this choice of u_0^- , $p^-(t)$ is an odd function, and it is monotonically increasing on $[t_0, -t_0]$, since $u^-(t) \sim u_0^-$ and $v^-(t) > 0$. Therefore,

$$t_2 = t_1 \quad \text{when } u_0^- = u_0. \quad (6.5)$$

This critical value, u_0 , of u_0^- is the dividing point between two distinct regimes. To leading order, formula (6.4) implies that

$$\text{if } u_0^- \begin{cases} < \\ > \end{cases} u_0, \text{ then } p_1 = -\gamma\sqrt{a} + \gamma \frac{3b\sqrt{b}}{u_0^-} \begin{cases} > \\ < \end{cases} 0. \quad (6.6)$$

Therefore, we also have:

$$t_2 \begin{cases} < \\ > \end{cases} t_1 \quad \text{when } u_0^- \begin{cases} < \\ > \end{cases} u_0. \quad (6.7)$$

The Implicit Function Theorem implies that the results of the above leading order calculation persist when the higher order terms are included, *i.e.* that there exists a critical value of u_0^- at $u_0 + \text{h.o.t}$. Combining formulae (6.5) and (6.7) gives precisely the statement of the proposition. \square

Remark 6.1. In this section we focus on the disappearance of the homoclinic one-pulse ($m = 1$). A similar analysis yielding the same result can be performed for the periodic patterns ($m > 1$): for $\beta = 1$ and b large enough singular periodic solutions exist, these solutions have disappeared when b has become ‘too small’.

6.2 Asymptotically large γ ($\beta > 1$)

In this section, we show that, when $\gamma \gg 1$ (with the requirement that $\delta^{2-\frac{1}{2}\beta} \ll 1$) the orbits $\Gamma^-(t)$ with $u_0^- = \mathcal{O}(1)$ cannot be forward asymptotic to S : there is no orbit Γ_1 homoclinic to S . We obtain this result by showing that neither t_1 nor t_2 exists for any $\mathcal{O}(1)$ value of u_0^- .

We start by recalling that at t_0 , the solution is given by $(u_0^-, p_0^-, v_0^-, q_0^-)$, where $p_0^- < 0$, while the other components are positive, and $\sqrt{(v_0^-)^2 + (q_0^-)^2} = \Delta$. We immediately see that, for $\gamma \gg 1$ and Δ small, there exists an $\epsilon_0 > 0$ such that for all $t > t_0 + \epsilon_0$, the u -component is negative ($u^-(t) < 0$) and the p -component remains negative. The existence of this ϵ_0 follows from the facts that $\gamma \gg 1$, $\dot{u} = \gamma p$, $\dot{p} = \gamma uv^2$ to leading order, and $(v_0^-)^2 \leq \Delta^2$, where Δ is small enough so that the u component must become negative before the p component can become positive. We remark that the larger one takes γ , the smaller ϵ_0 becomes. In addition, $u^-(t)$ and $p^-(t)$ are decreasing functions of time for $t > t_0 + \epsilon_0$.

Next, we observe that there is an $\mathcal{O}(1)$ constant $K > 0$ such that, at $t = t_0 + \epsilon_0$, we know

$$v_0^- - K\epsilon_0 \leq v^- \leq v_0^- + K\epsilon_0 \quad \text{and} \quad q^- \leq q_0^- + K\epsilon_0.$$

K is $\mathcal{O}(1)$, because the magnitude of the third and fourth components of the vector field (6.1) are $\mathcal{O}(1)$ and t_0 can be taken to be $\mathcal{O}(1)$ without loss of generality. Hence, using the second-order equation ($\ddot{v} = -uv^2 + bv$) for v obtained from the third and fourth components of (6.1), we also have $\ddot{v} > 0$ at $t = t_0 + \epsilon_0$.

Our goal is to show that neither t_1 nor t_2 exists. The nonexistence of t_2 follows from the fact that at $t = t_0 + \epsilon_0$ $u < 0$, $p < 0$ and $\dot{u} = \gamma p < 0$, $\dot{p} = \gamma uv^2 + \text{h.o.t.} < 0$; thus, $u < 0$, $p < 0$ for all $t \geq t_0$. Furthermore, this result also yields that $\ddot{v} = -uv^2 + bv > 0$ for all $t \geq t_0$, hence \ddot{v} remains positive for all $t > t_0 + \epsilon_0$. Both v and $\dot{v} (\equiv q)$ are positive at $t = t_0 + \epsilon_0$, thus, smoothness of solutions implies that q , and also v , cannot vanish before \ddot{v} does. We conclude that v and q remain positive for all $t > t_0 + \epsilon_0$, *i.e.*, that t_1 also does not exist.

Therefore, since the above argument applies to any arbitrary, positive, $\mathcal{O}(1)$ initial value u_0^- , we have obtained the desired result that neither t_1 nor t_2 exists for any u_0^- of $\mathcal{O}(1)$.

We conclude this section by extending the range of γ values for which the above result holds. In particular, the above arguments also apply when γ is $\mathcal{O}(1)$ but large, *i.e.*, they do not require γ to be asymptotically large. This conclusion follows directly from the facts that there again exists an ϵ_0 , since u^- again becomes negative while p^- remains negative when γ is large (and Δ is small), and one is again able to obtain the differential inequality for v .

6.3 $\gamma = \mathcal{O}(1)$ but small ($\beta \sim 1$)

In order to interpret the results for the equation (2.1) most directly from those of (6.1), we set $\delta^{1-\beta} = \gamma$ in (6.1) in this section. The vector field is now:

$$\begin{aligned} \dot{u} &= \gamma p \\ \dot{p} &= \gamma \left(uv^2 - \gamma^{\frac{1}{2}} \delta^{\frac{3}{2}} a + \gamma^{-1} \delta^3 au \right) \end{aligned}$$

$$\begin{aligned}\dot{v} &= q \\ \dot{q} &= -uv^2 + bv.\end{aligned}\tag{6.8}$$

We study the vector field (6.8) with $\gamma = \mathcal{O}(1)$.

The plane $\mathcal{M} \equiv \{(u, p, v, q) | v, q = 0\}$ is an invariant manifold of (6.8) for all $\gamma, \delta \geq 0$, and hence, in particular, for the case under consideration here, namely $\gamma = \mathcal{O}(1)$, but small. Theorems 3 and 4 from [9] imply that any compact subset of \mathcal{M} is a normally hyperbolic manifold with three-dimensional stable and unstable manifolds that are as smooth as the vector field, *i.e.*, C^r for every $r > 0$. It may be seen directly that the hypotheses of this theorem are satisfied, since the first Lyapunov type number is less than one along every trajectory on \mathcal{M} , the second Lyapunov type number is less than $1/r$ for all $r > 0$, and with the aid of bump functions on their boundaries, compact subsets of \mathcal{M} can be made overflowing (and inflowing) invariant. The vector field on \mathcal{M} is:

$$\begin{aligned}\dot{u} &= \gamma p \\ \dot{p} &= \gamma \left(-\gamma^{\frac{1}{2}} \delta^{\frac{3}{2}} a + \gamma^{-1} \delta^3 a u \right)\end{aligned}$$

The saddle point S is located at $(u = \gamma^{\frac{3}{2}} \delta^{-\frac{3}{2}}, p = 0)$, and its stable and unstable manifolds restricted to \mathcal{M} are given by $\ell^{s,u}$: $p = \pm \gamma^{-\frac{1}{2}} \delta^{\frac{3}{2}} \sqrt{a} (u - \gamma^{\frac{3}{2}} \delta^{-\frac{3}{2}})$. Hence, to leading order in δ : $p_0^- = \mp \gamma \sqrt{a}$.

First we note that t_1 must exist. This follows directly from the fact that $u(t_0) = u_0^- > 0$ and that $\dot{u} = \gamma p$ can be made as small as needed by adapting γ , thus by the equation $\ddot{v} = -uv^2 + bv$, $q = \dot{v}$ necessarily has a zero at $t = t_1$. As in section 6.1 we take $t_1 = 0$ without loss of generality. The main difficulty (relative to the case of $\gamma \ll 1$ considered in subsection 6.1) is that u is not constant to leading order, so that one cannot use formula (3.7) of [5] to compute $\frac{1}{2} \Delta p$, and hence to determine $p_1 \equiv p^-(0)$. Nevertheless, we can show that if u_0^- is sufficiently small, then $p_1 > 0$, while vice versa, if u_0^- is large, then $p_1 < 0$. Therefore, by continuous dependence of solutions on initial conditions and by the fact that the restricted unstable manifold of S is one-dimensional, there exists at least one $\mathcal{O}(1)$ value of u_0^- in between the small and large values such that for the solution $\Gamma^-(t)$ we have $p_1 = 0$. This solution is desired one-pulse orbit homoclinic to S due to the symmetry (6.2).

We begin with the exact computation (which uses the fourth component of the vector field (6.8) to substitute the uv^2 term):

$$p^-(t) = -\gamma \sqrt{a} + \int_{t_0}^t \dot{p}^-(s) ds + \text{h.o.t.} = \gamma \left[-\sqrt{a} + b \int_{t_0}^t v^-(s) ds - q^-(t) + q_0^- \right] + \text{h.o.t.}$$

Evaluation at $t = t_1 = 0$, where $q = 0$ by assumption, yields:

$$p_1 = \gamma \left[-\sqrt{a} + b \int_{t_0}^0 v^-(s) ds + q_0^- \right].\tag{6.9}$$

Note: if $\gamma \ll 1$ and $t_0 = -\infty$, then we recover the result of section 6.1, since the integral of $u^-(v^-)^2$ equals b times the integral of v^- in the $\delta \rightarrow 0$ limit, see section 2 or see [5], section 3.

We can now obtain the desired results that $p_1 > 0$ if u_0^- is small and $p_1 < 0$ if u_0^- is large. The general idea is, for example, that when u_0^- is sufficiently small, the integral of v^- will be large. First, $0 < q_0^- \leq k\Delta$ for some $0 < k \leq 1$. Hence, the third term on the right hand side of (6.9) is

small, and there exists a Δ such that $k\Delta < \sqrt{a}/10$. Next, one directly sees that $-\gamma^2\sqrt{a} < \dot{u} < 0$ as long as $p^-(t) < 0$. Hence,

$$u_0^- - \gamma^2\sqrt{a}(t - t_0) < u^-(t) < u_0^- \quad (6.10)$$

as long as $p^-(t) < 0$. (Note also that one can choose u_0^- and γ such that the lower bound remains positive, so that $p^-(t)$ increases.) Therefore, when u_0^- is sufficiently small, the solution $\Gamma^-(t)$ stays near the unstable subspace of the linear system $\dot{v} = q, \dot{q} = bv$ for a long time, and in fact, until $v^-(t)$ gets large. Moreover, from the estimate on $u^-(t)$, one sees that this closeness can be maintained for v as large as one pleases (before t reaches zero and q vanishes) by making u_0^- , and as necessary also γ , smaller. Hence, for sufficiently small u_0^- , the integral in (6.9) is large and $p_1 > 0$.

By contrast, by taking u_0^- sufficiently large, the integral can be made small, so that $p_1 < 0$. This follows again from the estimate on $u^-(t)$ but now the nonlinear term in \dot{q} dominates so that the integral can be made as small as desired by choosing u_0^- sufficiently large. \square

7 Numerical simulations

In this section, we compare the outcome of numerical simulations with the analytical results presented in sections 3–6. In subsection 7.1, we check the Hopf bifurcation values B_H (unscaled) or b_H and the pulse disappearance values B_D or b_D for the homoclinic one-pulse solutions ($m = 1$). Subsection 7.2 is devoted to spatially-periodic stationary states ($m > 1$).

Numerical simulations have been carried out using a moving grid code on the finite domain $[0, L]$ with either homogeneous Neumann boundary conditions or the Dirichlet boundary conditions $U = 1, V = 0$. Moreover, except where noted (*e.g.*, for studying periodic states), we only considered intervals that are long enough so that the boundaries are ‘far away’ and do not influence the dynamics. Detailed descriptions of the code we used are given in [3, 31], and a brief synopsis of the code and its application to the Gray-Scott model is given in section 6 of [5]. We also performed simulations using the code MOL1D, written by James M. Hyman.

7.1 The homoclinic one-pulse pattern ($m = 1$)

In this subsection, we report on a number of numerical experiments designed to concretely check the theoretically predicted value of $B_H(a; \delta) = b_H(a; \delta)\sqrt{\delta}$, the Hopf bifurcation point. In all simulations we performed near such a bifurcation point, we found that small perturbations of the homoclinic one-pulse induced a (temporally) periodic behavior of the pulse: it started to oscillate periodically up and down, without changing its position (in [5] such pulses were called ‘dancing pulses’). When B is such that the one-pulse was asymptotically stable ($B < B_H$), these oscillations damped out and the stationary one-pulse reappeared. For $B > B_H$, the oscillations become more and more violent until the one-pulse disappeared completely: the flow induced by (1.2) is attracted to the ‘trivial pattern’ ($U \equiv 1, V \equiv 0$). Thus, the Hopf bifurcation is apparently subcritical. In all the simulations we performed, the trivial pattern was found to be the only asymptotic attractor for $B > B_H$. This agrees with the asymptotic theory presented in section 5: the periodic patterns ($m > 1$) only become stable at $B_H(m) < B_H(m = 1)$, see (5.17) and section 7.2.

Furthermore, we numerically determined the value $B_D = b_D\delta$ at which the one-pulse ‘disappears’ (section 6) and splits into two traveling pulses ([29], [28], [5]).

First, we fixed a at $a = 1$ ($A = \delta^2$). We conducted numerical simulations of (1.2) with a series of sufficiently large interval length and number of grid points to check that the outcome of the simulations is independent of these quantities. We observed:

	δ^2	0.010	0.002	0.001	$\rightarrow 0$
	$\sqrt{\delta}$	0.32	0.21	0.18	$\rightarrow 0$
Hopf					
	$B_H(\delta)$	0.16	0.12	0.10	$\rightarrow 0$ as $\sqrt{\delta}$
	$b_H(\delta), \beta = \frac{1}{2}$	0.50	0.57	0.59	0.66
	$b_H(0) - b_H(\delta), \beta = \frac{1}{2}$	0.16	0.09	0.07	$\rightarrow 0$ as $\sqrt{\delta}$
Disappear					
	$B_D(\delta)$	0.07	0.03	0.02	$\rightarrow 0$ as δ
	$b_D(\delta), \beta = \frac{1}{2}$	0.21	0.15	0.12	$\rightarrow 0$ as $\sqrt{\delta}$
	$b_D(\delta), \beta = 1$	0.66	0.71	0.67	?

Thus, the simulations seem to agree with the predictions from the asymptotic theory: the values of the unscaled quantity $B_H(\delta)$ are of $\mathcal{O}(\sqrt{\delta})$. If we introduce the critical scaling, $\beta = \frac{1}{2}$, $B_H = b_H\sqrt{\delta}$, then we see that the values of $b_H(\delta)$ approach the theoretically predicted value of $b_H = b_H(0) \approx 0.66$ (at $a = 1$, (5.16)). Moreover, the error, $b_H(0) - b_H(\delta)$, is of the order, $\mathcal{O}(\sqrt{\delta})$, of the next terms in the asymptotic expansion.

The ‘splitting bifurcation’ at $B = B_D$, or $B_D = b_D\delta^\beta$, is considered in the last three rows of the above table. First we remark that the B -region in which the homoclinic one-pulse solution exists as a stable attractor $B \in (B_D(\delta), B_H(\delta))$ is rather small, *in the unscaled parameter B* : in [5] this region was called the ‘transition region’. Note that the asymptotic theory predicts that both $\lim_{\delta \rightarrow 0} B_D(\delta) = 0$ and $\lim_{\delta \rightarrow 0} B_H(\delta) = 0$. Thus, if we measure the width of this transition region in the unscaled parameter B , we find that it shrinks to zero in the limit $\delta \rightarrow 0$. However, if we introduce the critical scaling $B = b\sqrt{\delta}$ we observe that the b -interval in which the one-pulse is asymptotically stable approaches a non-zero value as δ decreases, as is predicted by the theory presented in sections 4 - 6. Moreover, we see that $b_D(\delta)$ is still of $\mathcal{O}(\sqrt{\delta})$ in the $\beta = \frac{1}{2}$ scaling. The theory of section 6 predicts that there exists a value of $B_D = \mathcal{O}(\delta)$ such that one-pulse solutions of the form given by Theorem 1 do not exist for $B < B_D = b_D\delta$. While we do not yet know of a quantitative mechanism to predict values of b_D (and hence the ? mark in the above table), the above reported numerical simulations seem to confirm that a disappearance value of B exists and that this value scales with δ .

Since the previous sections 4 and 5 give a rather detailed description of the Hopf bifurcation that takes place at $b = b_H$ ($\beta = \frac{1}{2}$), there are also other possibilities to validate this theory:

A second quantitative check on the theoretically predicted value of b_H can be obtained by measuring the period of the oscillations induced by the Hopf-bifurcation. We for instance fixed A at $A = \delta^2 a$, $a = 3.0$ and δ at $\delta^2 = 0.002$. The theory predicts that $b_H \approx 0.94$ ($\beta = \frac{1}{2}$, see (5.17)). Hence, the period of the oscillations near the Hopf bifurcation should be $T \approx 60$, because the analysis gives a scaled critical eigenvalue of $\hat{\lambda}_H \approx 0.53i$ at the bifurcation (5.16), which when

scaled back via $\lambda = b\delta^\beta \hat{\lambda}$ implies that the real $\lambda_H \approx 0.94 * (0.002)^{1/4} * (0.53)i \approx 0.105i$ so that the periodic part behaves approximately as $e^{0.105it}$. By comparison, near the critical value $B_H(\delta)$, $B_H(\delta) = b_H(\delta)\sqrt{\delta}$, we observed in the numerical simulation of (1.2) that the homoclinic one-pulse started to oscillate up and down. We measured the period of these oscillations to be ≈ 65 , which is in excellent agreement with the theoretical value.

The third set of numerical simulations, perhaps the most extensive, measures the critical scaling of b_H as a function of a . As demonstrated in section 5, the value of b_H is determined by formula (5.17) as a function m and a . Fixing the analysis on the homoclinic orbits ($m = 1$), we determined the theoretical formula for the critical scaling to be: $b_H(a) \approx 0.66\sqrt{a}$, for $m = \sigma = 1$, see (5.16). In order to verify this critical scaling numerically with homogeneous Neumann boundary conditions, we compared the theoretical $\{ th \}$ and numerical $\{ n \}$ values of $b_H(a)$:

		$L = 100, \delta^2 = 0.005$		$L = 200, \delta^2 = 0.002$	
a	$b_H \{ th \}$	$b_H \{ n \}$	$b_H/\sqrt{a} \{ n \}$	$b_H \{ n \}$	$b_H/\sqrt{a} \{ n \}$
0.5	0.47	0.39	0.55	0.38	0.54
1.0	0.66	0.54	0.54	0.56	0.56
1.5	0.81	0.64	0.52	0.68	0.55
2.0	0.93	0.73	0.52	0.78	0.55
2.5	1.04	0.80	0.51	0.87	0.55
3.0	1.14	0.87	0.50	0.94	0.54

Thus, once again, the numerical values agree with the theoretical values to approximately within the error of the next term, $\mathcal{O}(\sqrt{\delta})$, in the asymptotic expansion. In addition, the ratio $b_H(a)/\sqrt{a}$, which is also close to the leading order theoretical value of 0.66, appears to stay constant as a is changed, especially for the smaller value of δ . Therefore, the data corroborates the theoretical analysis of section 5 quite nicely.

Remark 7.1. Fixing a and δ , the size of the domain of attraction of the stable stationary one-pulse solutions depends on the value of $B \in (B_D, B_H)$. Near the boundaries of this interval we could only find stable solutions either by using initial data given by the explicit asymptotic formulae for Γ_1 (see section 2.1 and [5]) or by a continuation method. In the second case, we initially took B such that the one-pulse pattern could be found with the asymptotic formulae as initial conditions, then we took this pattern as initial condition and adapted B . If one uses more ‘crude’ initial conditions and does not apply the continuation method, then the region (B_D, B_H) shrinks significantly. This means that the domain of attraction of the one-pulse pattern becomes quite small, especially near B_D and B_H . Thus, one really needs to apply a continuation method to verify the correct behavior of B_D and B_H as functions of δ .

Remark 7.2. For several of the simulations reported in this subsection, we verified that the use of Neumann and Dirichlet boundary conditions gave qualitatively and quantitatively similar results. In all cases, the solutions were visually identical over approximately ninety percent of the domain. Disagreements occurred only near the boundaries.

Remark 7.3. As was already reported in [5], as δ^2 decreases it rapidly becomes impossible, given the hardware and software we used, to perform reliable simulations. For example, if the parameters are chosen to be $a = 1.0$, $\delta^2 = 0.0001$ and if the length of the interval is normalized to 1, we found

that the width of the stable V -pulse is ≈ 0.0005 . A reliable simulation needs at least about 100 grid points near the V -pulse, thus the moving grid code has to allocate about 100 grid points to an interval of width ≈ 0.0005 about the center of the pulse. This means that the distance between grid points becomes less than 10^{-6} .

7.2 Spatially periodic N -pulse patterns ($m > 1$)

In this section we discuss a number of observations on the stability of the periodic patterns. On finite intervals these patterns are called N -pulse patterns, where N denotes the number of singular (V)-pulses. First we note that now the length L of the interval plays a crucial role since it directly determines the period \mathcal{T} of an N -pulse pattern, *i.e.* $\mathcal{T} = \mathcal{T}(L, N)$. Note that the homogeneous Neumann boundary conditions and the symmetry of the solutions immediately yield that $\mathcal{T}(L, N) = \frac{L}{N+1}$, see also Figures 1, 7 and 8. Thus, by (2.10), L determines the value of m associated to such a pattern, and m is the key parameter that decides about the stability of a periodic pattern.

Since we performed a stability analysis on an unbounded domain, we should expect that the outcome of the numerical simulations differs from the predictions based on section 5. However, as long as we consider intervals of length $L \gg \mathcal{T}(m) \sim \frac{1}{\delta}$, the numerical simulations should, to leading order, agree with the theory developed in section 5, just as they did for the case $m = 1$ reported in section 7.1.

In the simulations reported in the table below, we fixed a at $a = 1$ and δ at $\delta^2 = 0.01$. Using periodic initial conditions and the continuation method, we determined for $N = 1, 2, \dots, 6$, $B_H = b_H(m)\sqrt{\delta}$, $B_D = b_D(m)\delta$ and the patterns appearing from the the N -pulse pattern as $B > B_H$ and $B < B_D$:

Number of pulses	N	1	2	3	4	5	6
Period \mathcal{T} , (2.10) \rightarrow	m	1.00	1.01	1.07	1.18	1.31	1.47
Hopf	$\beta = \frac{1}{2}$						
	$b_H(m)$	0.50	0.49	0.47	0.42	0.38	0.34
	$mb_H(m)$	0.50	0.50	0.50	0.50	0.50	0.50
	$b > b_H \rightarrow N$	0	1	1	2,3	4	4
Disappear	$\beta = \frac{1}{2}$						
	$b_D(m)$	0.21	0.21	0.19	0.17	0.15	0.13
	$\beta = 1$						
	$b_D(m)$	0.66	0.66	0.60	0.54	0.47	0.41
	$mb_D(m)$	0.66	0.66	0.64	0.63	0.62	0.60
	$b < b_D \rightarrow N$	4	4	6	8	10	12

The most striking outcome of these simulations is that mb_H remains constant, ≈ 0.50 , for $N = 1, 2, \dots, 6$! Of course, this is predicted by the asymptotic theory of section 5 ((5.15), (5.16)), but the extent to which it remains constant in these simulations is much higher than can be expected (note that theoretically $mb_H = 0.66$, see (5.16)). These observations also show that, for decreasing B , the first singular pattern to become stable is the homoclinic one-pulse and that $B_H(N_1) < B_H(N_2)$ if $N_1 > N_2$. This agrees with section 5 since $m(N_1) > m(N_2)$.

The value of B at the ‘splitting bifurcation’, $B = B_D$, again seems to scale with δ (see Remark 6.1). Since we do not know how to exactly determine b_D analytically, we also cannot predict the behavior of b_D as function of m . However, the numerical simulations suggest that, like $mb_H(m)$, $mb_D(m)$ remains constant to leading order.

The above table also shows that for a certain choice of $B = b\sqrt{\delta}$ various N -pulse patterns can be stable. For instance we see that the $N = 1, 2, 3$ patterns are stable for $\beta = \frac{1}{2}$ and $b = 0.45$ (and all others are unstable) – see Figures 1a and 7. Similarly, we found that for $\beta = \frac{1}{2}$ and $b = 0.19$ the N -pulse patterns with $N = 4, 5, \dots, 11$ are asymptotically stable, see Figures 1b and 8.

Furthermore, we also added information on the character of the pattern that appeared as an N -pulse pattern has become unstable (both for $B > B_H$ or for $B < B_D$). The behavior near B_H seems to be quite unpredictable and sensitive to perturbations: we could not discover a trend that enabled us to predict the number of pulses of the pattern that appeared after an N -pulse solution had become unstable by the Hopf bifurcation. Moreover, a priori negligible changes in the initial conditions, *i.e.* changes in the perturbation of the N -pulse pattern, can induce the evolution towards a different pattern: we have observed that the marginally unstable 4-pulse pattern either evolves into an 2-pulse pattern or into a 3-pulse pattern ($a = 1$, $b = 0.42$, $\beta = \frac{1}{2}$, $\delta^2 = 0.01$, $L = 100$). We did not analyze this behavior systematically. In Figure 9, we present a plot of the behavior of the grid as the 4-pulse solution has just become unstable: first two V -pulses disappear (after ‘dancing’ up and down), then the remaining 2 V -pulses slowly travel towards the stable 2-pulse configuration. Note that the oscillations of the grid are caused by the periodic subcritical Hopf behavior. The behavior near B_D is more clear: at the disappearance bifurcation, all pulses split simultaneously. The only subtlety is encountered for the one-pulse: initially, it splits into 2 pulses that travel towards the stationary 2-pulse configuration. However, since the b_D values of the one-pulse and the 2-pulse are so close (numerically), the 2-pulse usually also has to disappear: it also undergoes the dynamic splitting process. The final pattern is the stationary 4-pulse.

8 Discussion

The fact that for a given pair of parameter values ($A = a\delta^2$, $B = b\delta^\beta$) there may exist a m -interval of asymptotically stable $\mathcal{T}(m)$ -periodic solutions on the unbounded domain is reminiscent of the so-called Eckhaus instability criterion that appears throughout the literature on pattern formation, see [7] and [8]. In fact, there is a relation at least at the formal level: as was already noted in [5] the stable singular periodic pattern becomes a regular spatially periodic pattern as A increases, see especially Figure 10 in [5], where $A = \mathcal{O}(\delta)$. This periodic solution is the continuation of the periodic pattern that bifurcates from a ‘new’ trivial state ($U \equiv U_0, V \equiv V_0$) as A decreases through a certain $\mathcal{O}(1)$ value A_0 (this ‘new’ trivial state only exists for $4B^2 \leq A$, see also [27]). On the unbounded domain, this bifurcation can be described by a (real) Ginzburg-Landau equation, and thus one can (formally) conclude that there exists an interval of stationary, spatially periodic solutions for $0 < A_0 - A \ll 1$ with a subinterval of stable solutions [8]. Numerically one can continue this subinterval of bifurcated stable stationary, spatially periodic solutions into the interval of stable stationary, singular, spatially periodic solutions found in this paper.

Self-replication has also been studied in a number of other reaction-diffusion systems (the listing here is not exhaustive). These include a class of FitzHugh-Nagumo type models, see the Conclusion

section of [30], as well as the references there, for a discussion of some of these. See also the book [20] for a thorough, physically-based treatment of splitting in bistable models. The list of models that have been studied also includes a partially-linearized version of the Gray-Scott equations, where the reaction terms in the equation governing the inhibitor have been linearized, see [26].

Both the geometric methods used to construct the singular solutions for the Gray-Scott model (1.2) in [5] and the NLEP-approach to the stability of these solutions developed in this paper can in principle be applied to a large class of coupled reaction-diffusion equations of the form:

$$\begin{aligned}\delta^\rho \frac{\partial u}{\partial t} &= \frac{\partial^2 u}{\partial x^2} + \delta^2 F_1(u, v) + F_2(u, v) \\ \frac{\partial v}{\partial t} &= \delta^2 \frac{\partial^2 v}{\partial x^2} + G(u, v),\end{aligned}\tag{8.1}$$

where $\rho \geq 0$ and $\delta \ll 1$. Here, ρ plays the role of β in (1.2) (and $\beta = \frac{1}{2}$ corresponds to $\rho = 2$). Of course there are a number of conditions on the functions $F_i(u, v)$ and $G(u, v)$, for instance, one must have at least one homogeneous steady state $(u_*, 0)$ – corresponding to $(U \equiv 1, V \equiv 0)$ in (1.2) – which is a saddle-saddle fixed point of the time-independent system (8.1), so that the plane $\mathcal{M} = \{v = 0, v_x = 0\}$ is a normally hyperbolic invariant manifold. Due to the condition $F_2(u, 0) \equiv 0$ and to the factor of δ^2 in front of the F_1 term, the dynamics on this manifold is super slow, just as in the Gray-Scott model. Moreover, $G(u, v)$ must be such that the stationary fast reduced limit $0 = v_{\xi\xi} + G(u \equiv \text{const.}, v)$ has a homoclinic solution. The details of the analysis of this general system (8.1) will be the subject of future work. It should be noted that the model system studied and derived in [25] can be brought into the form (8.1); this system exhibits a self-replicating and multi-pulse behavior that is remarkably similar to that observed in the Gray-Scott model.

In addition to being generalizable to other systems with homoclinic orbits as discussed above, the theory can also be applied to systems with multiple saddle-saddle fixed points connected by fast heteroclinic orbits. These models can exhibit splitting phenomena similar to those of the FitzHugh-Nagumo or other bistable systems cited above.

Acknowledgements. The authors thank Paul Zegelung for teaching them how to use the software in [3, 31], as well as for a series of useful conversations. A.D. personally, and the authors collectively, gratefully acknowledge support from the Netherlands Organization for Scientific Research (NWO). R.G. gratefully acknowledges support from the National Science Foundation through grant DMS-9300848. T.K. gratefully acknowledges support from the National Science Foundation through CAREER grant DMS-9624471 and from the Alfred P. Sloan Foundation in the form of a Sloan Research Fellowship.

References

- [1] J. Alexander, R. A. Gardner, and C.K.R.T. Jones [1990], A topological invariant arising in the stability of travelling waves, *J. reine angew. Math.* **410**, 167–212.
- [2] K. Alhumaizi and R. Aris [1995], *Surveying a dynamical system: a study of the Gray-Scott reaction in a two-phase reactor*, Pitman Research Notes in Mathematics, vol. 341, Longman Scientific, Essex.
- [3] J.G. Blom, P.A. Zegeling [1994], Algorithm 731: A Moving-Grid Interface for Systems of One-Dimensional Time-Dependent Partial Differential Equations, *ACM Transactions in Mathematical Software*, **20**, 194–214.
- [4] A. Doelman, W. Eckhaus, and T.J. Kaper [1997], in preparation.
- [5] A. Doelman, T.J. Kaper, and P. Zegeling [1997], Pattern formation in the one-dimensional Gray-Scott model, *Nonlinearity*, **10**, 523–563.
- [6] A. Doelman, R. A. Gardner and T.J. Kaper [1997], Stability analysis of singular patterns in the 1-D Gray–Scott model II: Rigorous theory, in preparation.
- [7] W. Eckhaus [1965], *‘Studies in Nonlinear Stability Theory’*, Springer-Verlag, New York, etc.
- [8] W. Eckhaus [1992], On modulation equations of the Ginzburg-Landau type, in *ICIAM 91: Proc. 2nd Int. Conf. Ind. Appl. Math.* (R.E. O’Malley ed.), 83-98.
- [9] N. Fenichel [1971], Persistence and smoothness of invariant manifolds for flows, *Ind. Univ. Math. J.*, **21**, 193–226.
- [10] N. Fenichel [1979], Geometrical singular perturbation theory for ordinary differential equations, *J. Diff. Eq.*, **31**, 53–98.
- [11] R.A. Gardner [1993], On the structure of the spectra of periodic travelling waves, *J. Math. Pures Appl.*, **72**, 415–439.
- [12] R.A. Gardner [1997], Spectral analysis of long wavelength periodic waves and applications, to appear in *J. reine u. angew. Math.*
- [13] R.A. Gardner and C.K.R.T. Jones [1991], Stability of the travelling wave solutions of diffusive predator-prey systems, *Trans. AMS*, **327**, 465–524.
- [14] P. Gray and S.K. Scott [1983], Autocatalytic reactions in the isothermal, continuous stirred tank reactor: isolas and other forms of multistability, *Chem. Eng. Sci.*, **38**, 29–43.
- [15] P. Gray and S.K. Scott [1984], Autocatalytic reactions in the isothermal, continuous stirred tank reactor: oscillations and instabilities in the system $A + 2B \rightarrow 3B$, $B \rightarrow C$, *Chem. Eng. Sci.*, **39**, 1087–1097.
- [16] P. Gray and S.K. Scott [1985], Sustained oscillations and other exotic patterns of behavior in isothermal reactions, *J. Phys. Chem.*, **89**, 22–32.
- [17] D. Henry [1981], *Geometric theory of semilinear parabolic equations*, Lecture Notes in Mathematics, **840**, Springer-Verlag, New York.

- [18] C.K.R.T. Jones [1984], Stability of the travelling wave solution of the FitzHugh-Nagumo system, *Trans. AMS*, **286**, 431–469.
- [19] C.K.R.T. Jones [1995], Geometric singular perturbation theory, in *Dynamical systems, Montecatini Terme, 1994*, Lecture Notes in Mathematics, **1609**, R. Johnson (ed.), Springer-Verlag.
- [20] B.S. Kerner and V.V. Osipov [1994], *Autosolitons: a new approach to problems of self-organization and turbulence*, Kluwer, Dordrecht.
- [21] K.J. Lee and H.L. Swinney [1995], Lamellar structures and self-replicating spots in a reaction-diffusion system, *Phys. Rev. E*, **51**, 1899–1915.
- [22] K.-J. Lin, W.D. McCormick, J.E. Pearson, and H.L. Swinney [1994], Experimental observation of self-replicating spots in a reaction-diffusion system, *Nature*, **369**, issue no. 6477, 215–218.
- [23] MATHEMATICA^R, version 3.0 [1996], Wolfram Research, Inc.
- [24] P.M. Morse and H. Feshbach [1953], *Methods of Theoretical Physics*, McGraw-Hill, New York etc.
- [25] Y. Nishiura and D. Ueyama [1997], A skeleton structure for self-replication dynamics, *preprint*.
- [26] V.V. Osipov and A.V. Severtsev [1996], Theory of self-replication and granulation of spike autosolitons, *PLA*, **222**, 400–404.
- [27] J.E. Pearson [1993], Complex patterns in a simple system, *Science*, **261**, 189–192.
- [28] V. Petrov, S.K. Scott, and K. Showalter [1994], Excitability, wave reflection, and wave splitting in a cubic autocatalysis reaction-diffusion system, *Phil. Trans. Roy. Soc. Lond., Series A*, **347**, 631–642.
- [29] W.N. Reynolds, J.E. Pearson, and S. Ponce-Dawson [1994], Dynamics of self-replicating patterns in reaction diffusion systems, *Phys. Rev. Lett.*, **72**, 2797–2800.
- [30] W.N. Reynolds, S. Ponce-Dawson, and J.E. Pearson [1997], Self-replicating spots in reaction-diffusion systems, *Phys. Rev. E*, **56**, 185–198.
- [31] P.A. Zegeling, J.G. Verwer and J.C.H. v. Eijkeren [1992], Application of a Moving-Grid Method to a Class of 1D Brine Transport Problems in Porous Media, *International Journal for Numerical Methods in Fluids*, **15**, 175–191.

A Scaling analysis of the eigenvalue problem

As shown in section 3, the linear stability of the stationary solutions (U_0, V_0) is determined by the eigenvalue problem (3.2), which we copy here:

$$\begin{aligned}\lambda U &= \frac{d^2 U}{dx^2} - V_0^2 U - 2U_0 V_0 V - \delta^2 a U \\ \lambda V &= \delta^2 \frac{d^2 V}{dx^2} + V_0^2 U + 2U_0 V_0 V - b\delta^\beta V,\end{aligned}\tag{A.1}$$

with the ‘boundary conditions’ that U and V remain bounded as $x \rightarrow \pm\infty$. In order to study this eigenvalue problem, we introduced the relevant scalings for (U_0, V_0) from [5] (recall (2.2)):

$$x = \delta^{1-\frac{1}{2}\beta} \xi, U_0 = \delta^{\frac{3}{2}\beta} u_0, V_0 = \delta^{-\frac{1}{2}\beta} v_0,\tag{A.2}$$

Here, $\beta \in [0, 1)$. Also, as described in section 4, we introduced the following scalings for the eigenvalue and eigenfunctions:

$$\lambda = \delta^\ell b \tilde{\lambda}, \quad U = \delta^{\frac{3}{2}\beta} u, \quad \text{and} \quad V = \delta^{-\frac{1}{2}\beta} v \quad \text{for any } \ell \in \mathbf{R}.\tag{A.3}$$

We remark that $\tilde{\lambda}$ is assumed to be $\mathcal{O}(1)$ with these scalings. For convenience, U and V are scaled as U_0 and V_0 are scaled; however, there is no a priori reason to expect that u and v are $\mathcal{O}(1)$. In fact, u and v are not uniformly $\mathcal{O}(1)$ for all x for any choice of scaling, and so any convenient scaling will do. Inserting (A.2) and (A.3) into (A.1), one directly finds:

$$\begin{aligned}u_{\xi\xi} - \left(\delta^{2(1-\beta)} v_0^2 + \delta^{\ell+2-\beta} b \tilde{\lambda} + \delta^{4-\beta} a \right) u &= 2\delta^{2(1-\beta)} u_0 v_0 v \\ v_{\xi\xi} + \left(2u_0 v_0 - b - \delta^{\ell-\beta} b \tilde{\lambda} \right) v &= -v_0^2 u.\end{aligned}\tag{A.4}$$

In this appendix, we demonstrate that the significant scaling is $\ell = \beta$ so that unstable eigenvalues ($\text{Re}(\tilde{\lambda}) > 0$) might exist. Moreover, there is one additional significant scaling, $\ell = 1 - \beta$ (and $\ell \geq \beta$), in which there are eigenvalues with $\text{Re}(\tilde{\lambda}) > 0$, however, these eigenvalues are a subset of the eigenvalues found for the nonlocal eigenvalue problem at the ‘significant degeneration’ $\ell = \beta = 1 - \beta$, i.e. $\beta = \frac{1}{2}$. See Remark 5.3 and Figure 10.

First, we analyze the u equation. The three terms involving δ but not $\tilde{\lambda}$ are $\ll 1$, since $\beta \in [0, 1)$. The term involving both δ and $\tilde{\lambda}$, however, is only $\ll 1$ when $\ell > \beta - 2$. In fact, if instead $\ell \leq \beta - 2$ (see region A in Figure 10), and hence also $\ell - \beta < 0$, then the eigenvalue problem (A.4) becomes to leading order:

$$\begin{aligned}u_{\xi\xi} - \delta^{\ell+2-\beta} b \tilde{\lambda} u &= 0 \\ v_{\xi\xi} - \delta^{\ell-\beta} b \tilde{\lambda} v &= 0.\end{aligned}$$

This leading order eigenvalue problem has no solutions that are bounded both as $\xi \rightarrow \pm\infty$ when $\text{Re}(\tilde{\lambda}) > 0$. Therefore, there are no eigenvalues λ of (A.1) scaling with ℓ in region A; and, henceforth, we restrict our attention to the domain $\ell > \beta - 2$.

For all β, λ parameter combinations in this domain, we have:

$$u = \tilde{c} + \text{h.o.t}\tag{A.5}$$

during the fast regime, for some constant \tilde{c} . The constancy of u follows directly from the facts that $u_{\xi\xi} \ll 1$ and that terms linear in ξ grow without bound as $\xi \rightarrow \pm\infty$. The value of \tilde{c} is determined by matching the jump discontinuity in u_ξ in the slow and fast fields (recall Figure 3). There are two slow segments, one for each of the semi-infinite intervals $x < 0$ and $x > 0$. The jump discontinuity $\Delta_s U_x$ in the slow field at $x = 0$ between these two (rewritten in terms of the scaled variables) is:

$$\Delta_s u_\xi = -2\tilde{c}\sqrt{b\tilde{\lambda}\delta^{\frac{1}{2}\ell+1-\frac{1}{2}\beta}} + \text{h.o.t.}, \quad (\text{A.6})$$

for $\ell < 2$. This result is derived using the same procedure as employed in section 4.2: the leading order slow (outer) solutions are $U_\ell = c_\ell e^{\sqrt{b\delta^\ell\tilde{\lambda}+a\delta^2}x}$ for $x < 0$ and $U_r = c_r e^{-\sqrt{b\delta^\ell\tilde{\lambda}+a\delta^2}x}$ for $x > 0$, then by definition $\Delta_s U_x = \lim_{x \rightarrow 0^+} \frac{dU_r}{dx} - \lim_{x \rightarrow 0^-} \frac{dU_\ell}{dx}$, and finally (A.2) and (A.3) imply (A.6). We remark that, when $\ell = \beta$, the above formula is equivalent to (4.10). Also, for completeness, we remark that when $\ell > 2$, $\Delta_s u_\xi = -2\tilde{c}\sqrt{a}\delta^{2-\frac{1}{2}\beta} + \text{h.o.t.}$

The jump discontinuity $\Delta_f u_\xi$ in u_ξ in the fast field is given exactly by:

$$\Delta_f u_\xi = \int_{-\frac{T_f}{2}}^{\frac{T_f}{2}} u_{\xi\xi} d\xi,$$

where T_f is defined in section 4, and here we explicitly take $T_f = s \ln\left(\frac{1}{\delta}\right)$ for some s sufficiently large. By (A.4)(a) and (A.5),

$$\Delta_f u_\xi = \delta^{2(1-\beta)} \int_{-\frac{T_f}{2}}^{\frac{T_f}{2}} (\tilde{c}v_0^2 + 2u_0v_0v) d\xi + \delta^{\ell+2-\beta} b\tilde{\lambda}\tilde{c}T_f + \delta^{4-\beta} a\tilde{c}T_f + \text{h.o.t.} \quad (\text{A.7})$$

Now, the selection of the dominant term(s) in (A.7) depends on ℓ . In region B_1 , where $\beta - 2 < \ell \leq -\beta$ (see Figure 10), the term with $\tilde{\lambda}$ dominates and one can readily show that no eigenvalues λ with positive real part exist in this scaling. In fact, matching the values of the slow and fast jump discontinuities to leading order yields:

$$-2\tilde{c}\delta^{-\frac{\ell}{2}-1+\frac{1}{2}\beta} = \sqrt{b\tilde{\lambda}\tilde{c}}T_f.$$

Hence, either $\tilde{\lambda}$ is a function of δ (directly, as well as indirectly via T_f), or $\tilde{c} = 0$. The result in the former case contradicts the scaling hypothesis that $\tilde{\lambda}$ is independent of δ ; while in the latter case, the eigenvalue problem (A.4) becomes, to leading order:

$$v_{\xi\xi} - \delta^{\ell-\beta} b\tilde{\lambda}v = 0, \quad (\text{A.8})$$

which, when $\text{Re}(\tilde{\lambda}) > 0$, does not have solutions that are bounded both as $\xi \rightarrow \pm\infty$. Therefore, as claimed, there are no eigenvalues λ of (A.1) that scale with ℓ in region B_1 ; and, henceforth, we restrict our search even further to the domain in which $\ell > -\beta$.

In this domain, the dominant term in $\Delta_f u_\xi$ (see (A.7)) is the $\mathcal{O}(\delta^{2(1-\beta)})$ term involving the integral. Using the facts that $T_f = \mathcal{O}(s \ln\left(\frac{1}{\delta}\right))$ for s sufficiently large, and that $v_0 \rightarrow 0$ exponentially fast as $\xi \rightarrow \pm\infty$, one sees directly that the leading order asymptotics for $\Delta_f u_\xi$ is given by:

$$\Delta_f u_\xi = \delta^{2(1-\beta)} \int_{-\infty}^{\infty} (\tilde{c}v_0^2 + 2u_0v_0v) d\xi. \quad (\text{A.9})$$

(The tails are $\frac{1}{K}e^{-\frac{KT_f}{2}} = \mathcal{O}(\delta^{\frac{Ks}{2}})$ for some $K > 0$, and hence they are of higher order than the neglected terms.) Matching this leading order fast jump discontinuity $\Delta_f u_\xi$ given by (A.9) to that of the slow field $\Delta_s u_\xi$ given by (A.6), one obtains:

$$\delta^{2(1-\beta)} \int_{-\infty}^{\infty} (\tilde{c}v_0^2 + 2u_0v_0v) d\xi = -2\tilde{c}\sqrt{b\tilde{\lambda}}\delta^{\frac{\ell}{2}+1-\frac{1}{2}\beta}. \quad (\text{A.10})$$

This matching result immediately yields

$$\tilde{c} = \frac{-\delta^{1-\frac{3}{2}\beta-\frac{1}{2}\ell}u_0^3}{\sqrt{b\tilde{\lambda}}u_0^2 + 3\delta^{1-\frac{3}{2}\beta-\frac{1}{2}\ell}b\sqrt{b}} \int_{-\infty}^{\infty} v_0v d\xi. \quad (\text{A.11})$$

Remark A.1. We used the result $\int_{-\infty}^{\infty} v_0^2 d\xi = (6b\sqrt{b})/u_0^2$ that follows directly from section 2, see also [5]. Moreover, when $\ell = \beta$, the formula (A.11) reduces to that for \tilde{c} obtained in section 4.3.

The remainder of the information we will need in this section is contained in the equations (A.11) for \tilde{c} and (A.4) (with (A.5)) for v . In particular, these equations determine two transition lines:

$$\begin{aligned} L_1 : \ell &= 2 - 3\beta \\ L_2 : \ell &= \beta \end{aligned} \quad (\text{A.12})$$

that are central to the analysis. Along and above L_1 , $\tilde{c} = \mathcal{O}(1)$; while $\tilde{c} \ll 1$ below L_1 . In addition, along L_2 , a transition occurs in which the asymptotic ordering of the eigenvalue term in the v equation goes from $\gg 1$ below L_2 to $\mathcal{O}(1)$ on L_2 , to $\ll 1$ above L_2 . The scaling along L_2 is the significant one studied in sections 3-6. Moreover, the transition point along L_2 at $\beta = 1/2$ where L_1 and L_2 intersect has been given special attention in sections 3-6.

The lines L_1 and L_2 separate the domain $\ell > -\beta$ that we are studying into four regions B_2 , B_3 , D_1 , and D_2 (see Figure 10). In both B_2 and B_3 , the eigenvalue term in the v equation is $\gg 1$, as stated above; while the right hand side is $\ll 1$ in B_2 and $\mathcal{O}(1)$ in B_3 , because $\ell < 2 - 3\beta$ and $\ell > 2 - 3\beta$, respectively, in these domains. Hence, to leading order, the eigenvalue problem (A.4) in both regions is also given by (A.8). Therefore, for all $\beta \in [0, 1)$, the same argument as applied in the region B_1 demonstrates that there are no eigenvalues λ of (A.1) with positive real part that scale with ℓ in regions B_2 and B_3 .

Region D_1 is given by $\beta < \ell \leq 2 - 3\beta$. The eigenvalue problem (A.4) becomes:

$$v_{\xi\xi} + \left(2u_0v_0 - b - \delta^{\ell-\beta}b\tilde{\lambda}v\right)v = -\delta^{1-\frac{3}{2}\beta-\frac{1}{2}\ell}\tilde{c}'v_0^2, \quad (\text{A.13})$$

where $\tilde{c} = \delta^{1-\frac{3}{2}\beta-\frac{1}{2}\ell}\tilde{c}' \leq \mathcal{O}(1)$ and $\tilde{c}' = \mathcal{O}(1)$ throughout D_1 , see (A.11). This problem is similar to (4.3), with $\hat{\lambda}$ replaced by $\delta^{\ell-\beta}\tilde{\lambda}$ and \hat{c} replaced by $\delta^{1-\frac{3}{2}\beta-\frac{1}{2}\ell}\tilde{c}'$. Thus, solutions to (A.13) correspond to solutions to (4.3) with $|\hat{\lambda}| \ll 1$. More precisely, (by comparing (A.11) to (4.12)): (A.13) can be brought into the form (5.2) with, by (5.1),

$$P^2 = 4(1 + \delta^{\ell-\beta}\tilde{\lambda}) \quad \text{and} \quad C = \frac{9}{1 + 3\frac{b^2m^2}{a}\delta^{\beta+\ell-1}\sqrt{\tilde{\lambda}}}, \quad (\text{A.14})$$

since here $\sigma = \delta^{1-\frac{3}{2}\beta-\frac{1}{2}\ell}$. Thus, in this case, relation (5.15) reduces to

$$b^2 = \frac{a}{3m^2} \delta^{\beta+\ell-1} \frac{1}{\sqrt{\tilde{\lambda}}}, \quad (\text{A.15})$$

at leading order, since $\lim_{P \rightarrow 2} C(P) = \frac{9}{2}$ (5.14). By construction, $b, \tilde{\lambda} = \mathcal{O}(1)$; thus, (A.15) can only have solutions if $\ell = 1 - \beta$ (and $\ell \geq \beta$), see Figure 10.

Thus, only on the line segment $\ell = 1 - \beta$ with $\beta \leq \ell \leq 1$ do there exist (real, positive) eigenvalues in the region D_1 . Note that these eigenvalues correspond to the small eigenvalues $0 < \hat{\lambda} \ll 1$ found in section 5 for $\ell = \beta = \frac{1}{2}$ and $b \gg 1$.

Finally, we show that in region D_2 , which corresponds to $\ell > \beta$, $\ell > 2 - 3\beta$, there do not exist eigenvalues with positive real parts and with $\tilde{\lambda} = \mathcal{O}(1)$. The eigenvalue problem (A.4) is, to leading order:

$$v_{\xi\xi} + (2u_0v_0 - b)v = -\tilde{c}v_0^2 + \delta^{\ell-\beta}b\tilde{\lambda}v, \quad (\text{A.16})$$

where $\tilde{c} = \mathcal{O}(1)$ throughout D_2 , because D_2 lies above L_1 . This property of \tilde{c} is what makes the result for D_2 differ from that for D_1 . More precisely, to leading order, we have:

$$\tilde{c} = \frac{u_0^3 \int_{-\infty}^{\infty} v_0 v d\xi}{3b\sqrt{b}}. \quad (\text{A.17})$$

Therefore, the leading order eigenvalue problem (A.16) is precisely (4.13) with $\lambda = 0$, and from the analysis in section 5, we may directly conclude that there does not exist a solution to this problem with b finite. See also Figure 5. Hence, the full eigenvalue problem cannot be solved.

The results of this appendix are summarized in Figure 10. This figure shows that there are only two line segments in the (β, ℓ) -strip, $\ell = \beta$ and $\ell = 1 - \beta$ with $\beta \in [0, \frac{1}{2}]$, in which there exist unstable eigenvalues. The crucial case $\beta = \frac{1}{2}$ – sections 4 and 5 – occurs here as the intersection of the two line-intervals.

Figure Captions

Figure 1. Stationary one-pulse solutions and spatially periodic stationary solutions of (1.2) observed in numerical simulations with $\delta^2 = 0.01$ and $L = 100$: (a) $a = 1$, $b = 0.45$, $\beta = \frac{1}{2}$; (b) $a = 1$, $b = 0.19$, $\beta = \frac{1}{2}$. In these plots, as well as in all other plots, the concentration V is given by the solid curves with nearly zero vertical intercept, containing the high and narrow spikes, while the concentration U is given by the solid curve whose vertical intercept is higher, and which has local minima at the center of the V -pulses.

Figure 2. Schematic illustrations of (a) the one-pulse homoclinic orbit $\Gamma_1(\xi)$ and (b) a singular periodic orbit $\Gamma_m(\xi)$, $m > 1$, in the 4-d phase space of (2.1). Note that these schematic illustrations show the slow segments in (u_ξ, u) coordinates and the fast segments in $(v, -v_\xi)$ coordinates.

Figure 3. The singular structure of a solution $U(x)$ of (3.2) as function of the slow variable x .

Figure 4. A plot of $C(P)$ as function of $P \in [2, 4]$ (5.12).

Figure 5. The solution $b = b(\hat{\lambda}; a, \sigma, m)$ of (5.15) as function of $\text{Re}(\hat{\lambda})$ for $a = \sigma = 1$ (middle curve), $\frac{\sqrt{a\sigma}}{m} \gg 1$ (top curve) and $\frac{\sqrt{a\sigma}}{m} \ll 1$ (bottom curve). Note that $b_H(1, 1, 1) \approx 0.66$ and $b_c(1, 1, 1) \approx 0.99$.

Figure 6. The ‘pitchfork-orbit’ through the complex plane of the two unstable eigenvalues $\hat{\lambda}_{1,2} = \hat{\lambda}_{1,2}(b)$ of the NLEP (4.14) for decreasing b (and $a = \sigma = m = 1$); $\hat{\lambda}_1 \approx 0$, $\hat{\lambda}_2 \approx \frac{5}{4}$ for $b \gg 1$, $\hat{\lambda}_1 = \hat{\lambda}_2 \approx 0.30$ for $b = b_c(1, 1, 1) \approx 0.99$, $\hat{\lambda}_1 = -\hat{\lambda}_2 \approx 0.53i$ for $b = b_H(1, 1, 1) \approx 0.66$.

Figure 7. $a = 1$, $b = 0.45$, $\beta = \frac{1}{2}$: the 1, 2, 3-pulse solutions are stable: (a) the 2-pulse solution; (b) the 3-pulse solution. The stable one-pulse solution is shown in Figure 1a. Here $\delta^2 = 0.01$ and $L = 100$.

Figure 8. $a = 1$, $b = 0.19$, $\beta = \frac{1}{2}$: the 4, 5, ..., 11-pulse solutions are stable: (a) the 4-pulse solution; (b) the 11-pulse solution. The stable 7-pulse solution is shown in Figure 1b. Here also $\delta^2 = 0.01$ and $L = 100$.

Figure 9. (a) An $x(t)$ vs. t plot of the behavior of the grid points in the case that the 4-pulse solution loses its stability due to the Hopf-bifurcation ($a = 1$, $b = 0.42$, $\beta = \frac{1}{2}$, $\delta^2 = 0.01$, $L = 100$). The V -pulses ‘dance’ up and down, with increasing amplitude, and this causes the periodic grid oscillations. Two V pulses ‘shrink’ to $V = 0$ at $T \approx 3100$. The two remaining pulses travel (very) slowly towards the asymptotically stable periodic 2-pulse: in (b) $(U(x, T), V(x, T))$ is shown (see the solid curve with the two pulses with the smaller maximum in V) for $T = 3200$, *i.e.* just after the disappearance of the two pulses, and for $T = 13200$: the pattern has evolved towards the 2-pulse attractor (the solid curves with the symmetric U and V profiles).

Figure 10. The six regions in the $\beta - \ell$ plane analyzed in Appendix A and the line-intervals $\ell = \beta$, $\beta \in [0, 1)$ and $\ell = 1 - \beta$, $\beta \in [0, \frac{1}{2}]$.

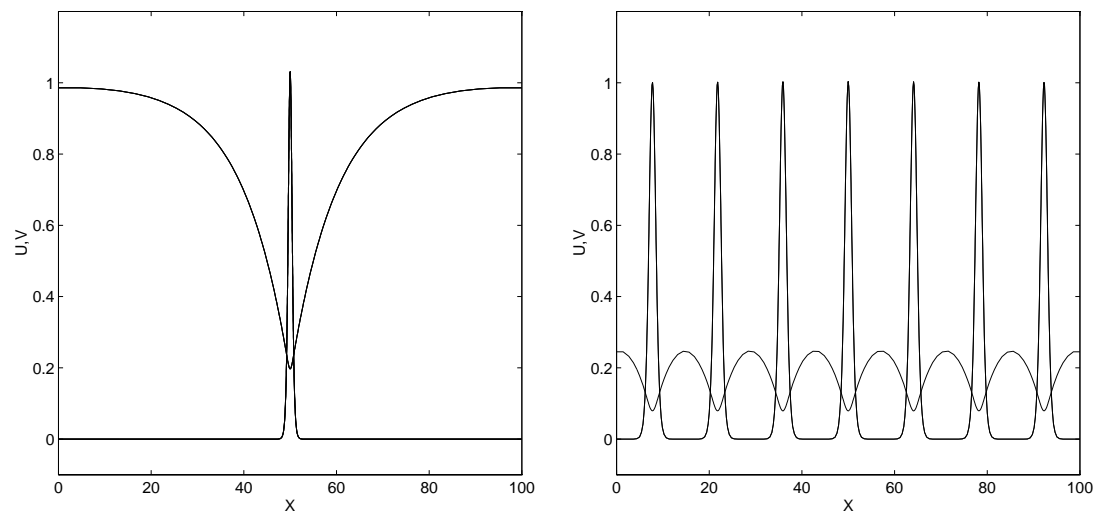


Figure 1:

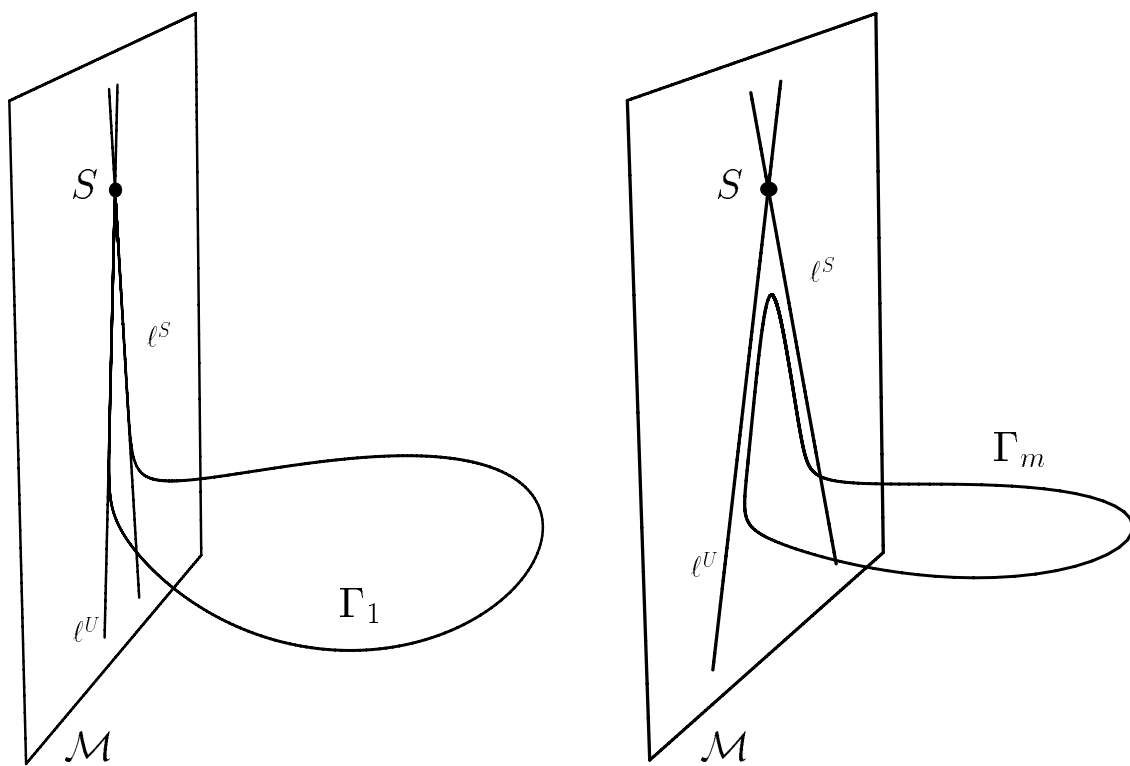


Figure 2:

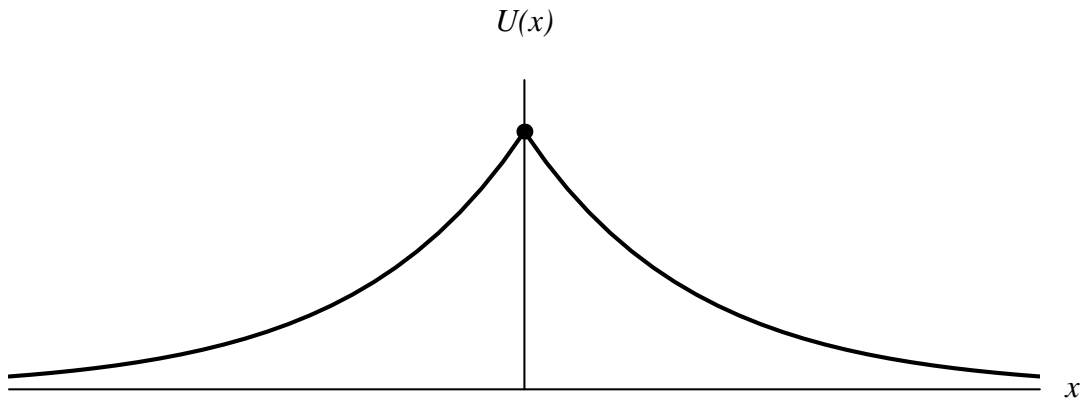


Figure 3:

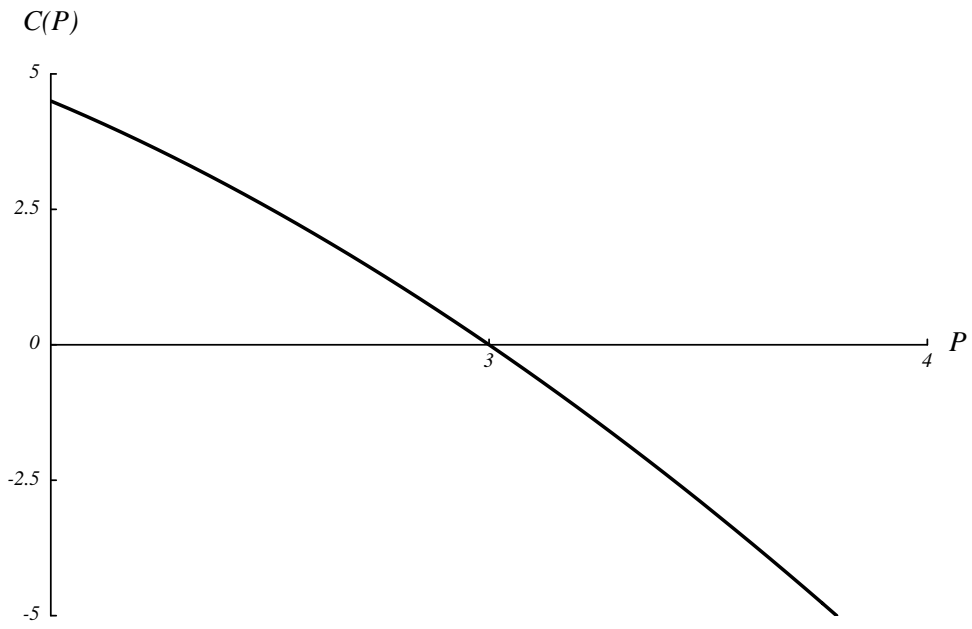


Figure 4:

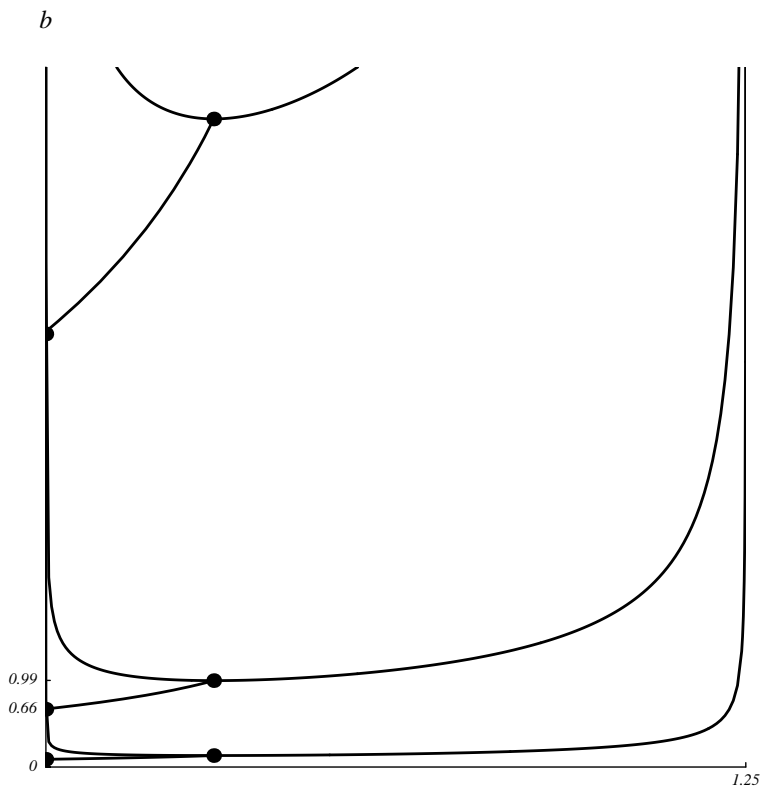


Figure 5:

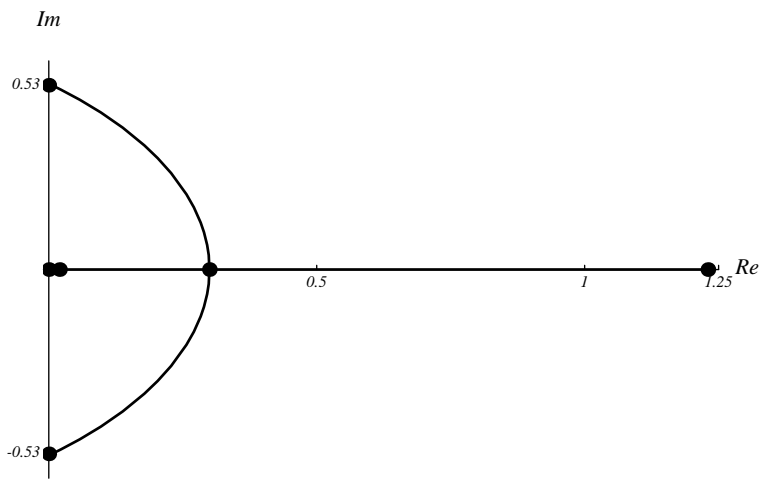


Figure 6:

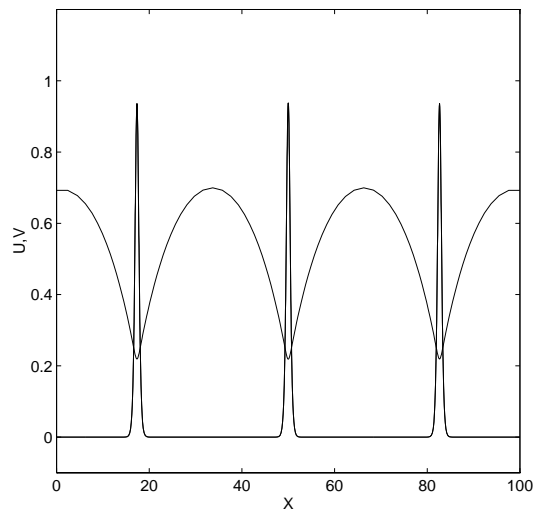
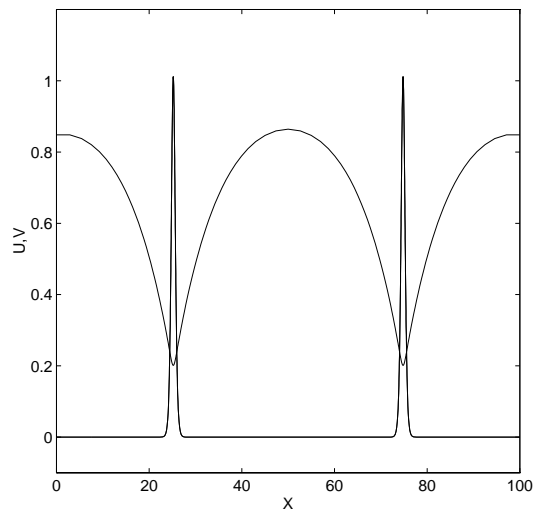


Figure 7:

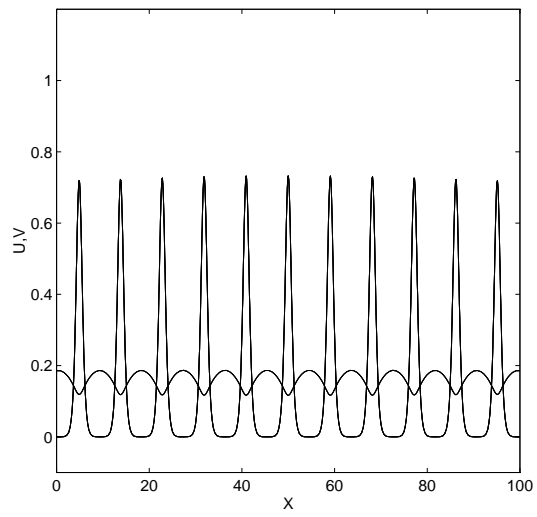
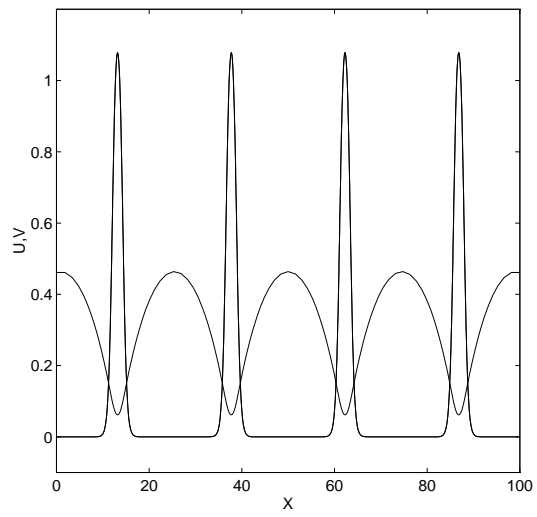


Figure 8:

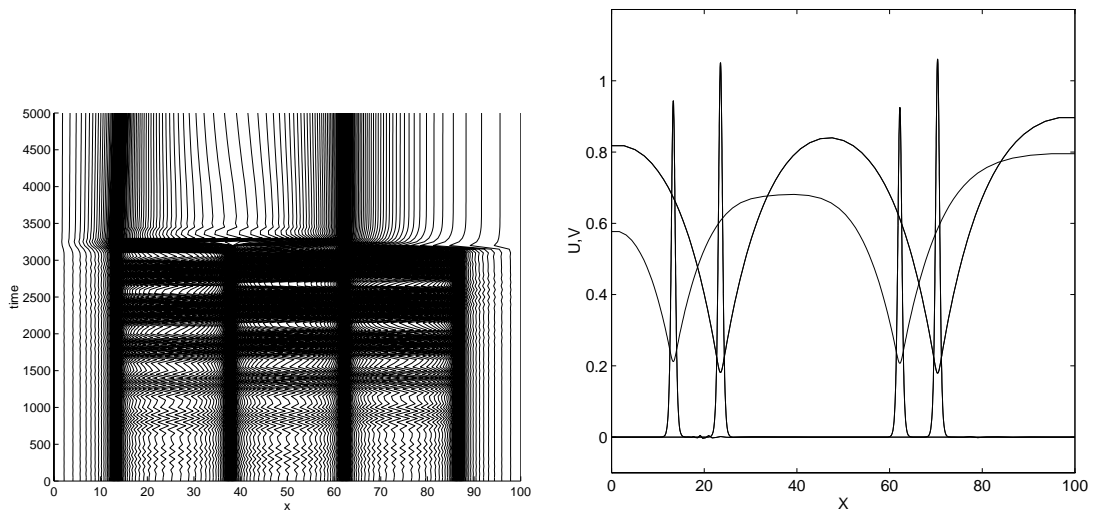


Figure 9:

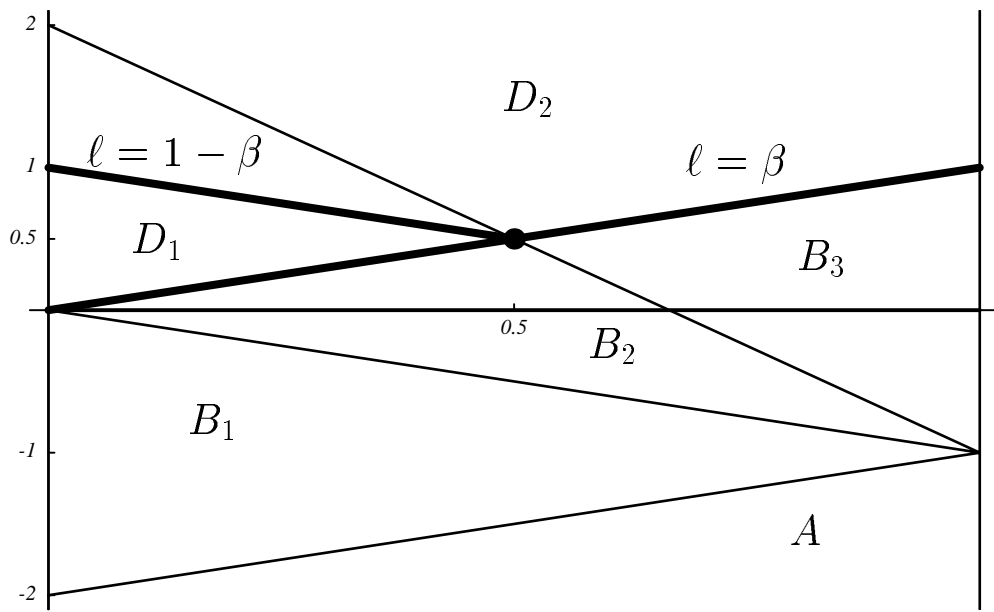


Figure 10: